

Measurement of Human Pilot Dynamic Characteristics in Flight Simulation

by

FINAL REPORT

JAMES T. REEDY
B.S. (California State University, Sacramento) 1985

THESIS

Submitted in partial satisfaction of the requirements for the degree of

MASTER OF SCIENCE

in

Mechanical Engineering

in the

GRADUATE DIVISION

of the

UNIVERSITY OF CALIFORNIA

DAVIS

Approved:

Ronald O. Hess
.....
Dean Karnopp
.....
John Grewey
.....

Committee in Charge

Deposited in the University Library

.....
Date

.....
Librarian

MAY 31 1986

CASI

Acknowledgements

This research was sponsored by the NASA Ames Research Center, Dryden Flight Research Facility grant number NCC2-241. Mr. Donald T. Berry was the contact monitor. I would like to thank Edwin W. Aiken and Michelle M. Eshow of the Flight Dynamics and Controls Branch at NASA Ames Research Center for their participation in the experiment and the acquisition of data that made this project possible. I would also like to thank Professor Ronald A. Hess of the University of California, Davis for his time, support and guidance.

Abstract

Fast Fourier Transform (FFT) and Least Square Error (LSE) estimation techniques were applied to the problem of identifying pilot-vehicle dynamic characteristics in flight simulation. A brief investigation of the effects of noise, input bandwidth and system delay upon the FFT and LSE techniques was undertaken using synthetic data. Data from a piloted simulation conducted at NASA Ames Research Center was then analyzed. The simulation was performed in the NASA Ames Research Center Variable Stability CH-47B helicopter operating in fixed-basis simulator mode. The piloting task consisted of maintaining the simulated vehicle over a moving hover pad whose motion was described by a random-appearing sum of sinusoids. The two test subjects used a head-down, color cathode ray tube (CRT) display for guidance and control information. Test configurations differed in the number of axes being controlled by the pilot (longitudinal only versus longitudinal and lateral), and in the presence or absence of an important display indicator called an "acceleration ball". A number of different pilot-vehicle transfer functions were measured, and where appropriate, qualitatively compared with theoretical pilot-vehicle models. Some indirect evidence suggesting pursuit behavior on the part of the test subjects is discussed.

Table of Contents

Title page -----	i
Acknowledgements -----	ii
Abstract -----	iii
Table of Contents -----	iv
List of Tables -----	v
List of Figures -----	vii
List of Programs -----	ix
1.0 Introduction -----	1
2.0 Background -----	2
2.1 Brief Review of Techniques for Human Transfer Function Estimation -----	2
2.2 Least Squares and Sum of Sines - Hess/Mnich -----	6
2.3 Description of the Reedy Identification - Similarity to NIPIP -----	11
2.4 Example Cases; Noise Effects, Input Bandwidth Effects, Delay Estimation Techniques -----	14
3.0 A Multi-Axis Manned Simulation Task -----	17
4.0 Conclusions -----	24
5.0 References -----	25
6.0 Appendix I Tables -----	27
7.0 Appendix II Figures -----	52
8.0 Appendix III Computer Programs -----	74

List of Tables - Appendix I

Number	Title	Page
1.	Z-transforms of physical systems	28
2.	Noise and cutoff frequency comparison	29
3.	Bias comparison	30
4.	Identification with delay comparison	31
5.	Identified delay comparison	32
6.	Open-loop vs. closed-loop comparison	33
7.	Sum of sines input	34
8.	Multi-loop helicopter simulation comparison	35
9.	Longitudinal sum of sines for the CH-47B helicopter	36
10.	Lateral sum of sines for the CH-47B helicopter	37
11.	X/Xpad TF. ID. results for subject 1, longitudinal tracking only	38
12.	X/Xpad TF. ID. results for subject 2, longitudinal tracking only	39
13.	X/Xpad TF. ID. results for subject 1, lateral and longitudinal tracking	40
14.	X/Xpad TF. ID. results for subject 2, lateral and longitudinal tracking	41
15.	X/Xpad TF. ID. results for subject 1, lateral and longitudinal tracking without the acceleration symbol	42
16.	X/Xpad TF. ID. results for subject 2, lateral and longitudinal tracking without the acceleration symbol	43
17.	Xball/Xpad TF. ID. results for subject 1, longitudinal tracking only	44
18.	Xball/Xpad TF. ID. results for subject 2, longitudinal tracking only	45
19.	Xball/Xpad TF. ID. results for subject 1, lateral and longitudinal tracking	46
20.	Xball/Xpad TF. ID. results for subject 2, lateral and longitudinal tracking	47
21.	Xball/Xball error TF. ID. results for subject 1, longitudinal tracking only	48
22.	Xball/Xball error TF. ID. results for subject 2, longitudinal tracking only	49
23.	Xball/Xball error TF. ID. results for subject 1, lateral and longitudinal tracking	50

24. Xball/Xball error TF. ID. results for subject 2,
lateral and longitudinal tracking

51

List of Figures - Appendix II

Number	Title	Page
1.	Open-loop block diagram	53
2.	Closed-loop block diagram	53
3.	Closed-loop block diagram with noise	53
4.	Closed-loop block diagram with noise and bias	53
5.	Multi-loop hovering helicopter model block diagram	53
6.	Noise comparison, medium cutoff frequency	54
7.	Bias comparison, medium cutoff frequency	54
8.	Delay comparison, medium cutoff frequency	55
9.	Open-loop frequency cutoff comparison, zero noise	55
10.	Closed-loop cutoff comparison, zero noise	56
11.	Closed-loop cutoff comparison with noise	56
12.	Open-loop vs. closed-loop with step input	57
13.	Open-loop vs. closed-loop with medium cutoff sum of sines input	57
14.	FFT vs. LSE, open-loop, with medium cutoff sum of sines input	58
15.	FFT vs. LSE, closed-loop with medium cutoff sum of sines input	58
16.	Multi-loop FFT vs. LSE with bias, and zero noise	59
17.	Multi-loop FFT vs. LSE with noise and bias	59
18.	Display symbology for the CH-47B helicopter	60
19.	Hypothesized pilot loop closures with acceleration ball display symbology	60
20.	X/Xpad TF. ID. for subject 1, longitudinal tracking only	61
21.	X/Xpad TF. ID. for subject 2, longitudinal tracking only	62
22.	X/Xpad TF. ID. for subject 1, lateral and longitudinal tracking	63
23.	X/Xpad TF. ID. for subject 2, lateral and longitudinal tracking	64
24.	X/Xpad TF. ID. for subject 1, lateral and longitudinal tracking without the acceleration symbol	65
25.	X/Xpad TF. ID. for subject 2, lateral and longitudinal tracking without the acceleration symbol	66

26.	X position vs. time plot for X/Xpad, subject 1, lateral and longitudinal tracking	67
27.	X position vs. time plot for X/Xpad, subject 1, lateral and longitudinal tracking without the acceleration symbol	67
28.	Xball/Xball error TF. ID. for subject 1, longitudinal tracking only	68
29.	Xball/Xball error TF. ID. for subject 2, longitudinal tracking only	68
30.	Xball/Xball error TF. ID. for subject 1, lateral and longitudinal tracking	69
31.	Xball/Xball error TF. ID. for subject 2, lateral and longitudinal tracking	69
32.	Alternate multi-loop pilot loop closures with acceleration ball display symbology	70
33.	Xball/Xpad TF. ID. for subject 1, longitudinal tracking only	71
34.	Xball/Xpad TF. ID. for subject 2, longitudinal tracking only	71
35.	Xball/Xpad TF. ID. for subject 1, lateral and longitudinal tracking	72
36.	Xball/Xpad TF. ID. for subject 2, lateral and longitudinal tracking	72
37.	Xball/Xpad TF. for compensatory pilot behavior	73

List of Programs - Appendix III

Number	Title	Page
1	ACSL multi-loop helicopter simulation	75
2	ACSL closed loop simulation, sum of sines input with noise, delay, and bias	77
3	ACSL closed loop simulation, sum of sines input with noise, and delay	78
4	ACSL closed loop simulation, sum of sines input with noise	79
5	ACSL closed loop simulation, sum of sines input	80
6	Z-domain to W'-domain transformation subroutine	81
7	Fast Fourier Transform subroutine	83
8	LSE identification using model 8, no delay with bias	85
9	LSE identification using model 8 with a 3 time constant delay	86
10	LSE identification using model 8	87
11	LSE identification using model 9	88

1.0 Introduction

A pilot when combined with a modern aircraft, whether an airplane or helicopter, forms one of the most complicated systems to be analyzed by a control engineer. Once the basic problem of stability is solved, the issue of handling qualities can be raised. In order to improve handling qualities, a better integration of man and machine is required, and in order to achieve better man machine integration, the system dynamics must be evaluated and optimized. The first step in this process is the measurement of the vehicle and pilot dynamics. The measurement of human dynamics is complicated by the fact that human characteristics are task dependent. Their dynamics can change dramatically depending upon the type of task being performed, and their familiarity with it. Dynamics can also vary between pilots for the same task.

Early work in the area of human pilot dynamics (e.g. ref. 1) has led to the formation of a vast data base, which has aided many researchers in their development of models of the human pilot. Over the past three decades, many models have been proposed and tested. Models varying in complexity from the Crossover Model for single loop systems to the Structural Isomorphic Model. Although the crossover model is the simplest, it is the most general. When expressed mathematically the crossover model appears as,

$$Y_p Y_c = \frac{K_p K_c e^{-ts}}{S} = \frac{\omega_c e^{-ts}}{S} \quad (1)$$

where Y_p is the pilot transfer function, Y_c is the plant transfer function, K_p and K_c are gains, τ is the system time delay, and ω_c is the crossover frequency. This model states that no matter what the plant dynamics, the operator compensates for them and the system crossover model is preserved. As the name implies this model is accurate near the crossover frequency, but if the low or high frequencies are important a different model must be used. The precision model for single loop systems (ref. 2) is accurate for a broader frequency range than the crossover model. If a more complicated model is required there are several multiloop examples to choose from. The McRuer Structural Isomorphic Model (ref. 2), the Linear Optimal Control Model (ref. 3), and the Hess Structural Model (ref. 4) are three options available.

This paper uses simple single-loop models for generation of data that is used to test the least squares identification process and the Fast Fourier Transform analysis. Once the simple models were identified properly, a more complicated multiloop example was exercised. After the multiloop example was completed the identification procedure was used to identify vehicle pilot dynamics from data obtained from a CH-47B helicopter at the NASA Ames Research Center.

2.0 Background

2.1 Brief review of techniques for human transfer function estimation.

When deciding upon an identification technique there are many choices, and depending on the system being identified there will be

advantages to using one method over another. Some of the different methods used employ orthogonal filters, spectral analysis techniques including Fast Fourier Transforms, and least squares estimation.

The orthogonal filter method is a generalized technique that models the system dynamics as a series of transfer functions or linearly independent filters. The set of linearly independent filters are of the form

$$G(j\omega) = e^{-\lambda j\omega} \left[\frac{\beta_1}{\tau_1 j\omega + 1} + \frac{\beta_2 (\tau_1 j\omega - 1)}{(\tau_1 j\omega + 1)(\tau_2 j\omega + 1)} + \dots \right] \quad (2)$$

where β_1, β_2, \dots are determined by a regression technique, and τ_1, τ_2, \dots are predetermined time constants. The time constants are selected from models of the pilot that include the sensory organs, muscular mechanics, and the feedback therein. (see ref. 5 pg.4) Although general, the results from the orthogonal filter method are somewhat difficult to interpret due to the many parameters in the model.

Power and cross power spectral densities can be computed to determine the pilot dynamics using spectral measurement techniques. The power spectral density of a random signal $x(t)$ is derived from the autocorrelation function

$$\Phi_{xx}(\tau) = \lim_{T \rightarrow \infty} \frac{1}{2T} \int_{-T}^T x(t)x(t+\tau) dt \quad (3)$$

which can also be defined as one half of a Fourier Transform pair

$$\Phi_{xx}(\tau) = \frac{1}{2\pi} \int_{-\infty}^{\infty} \Phi_{xx}(\omega) e^{j\omega\tau} d\omega \quad (4)$$

where $\Phi_{xx}(\omega)$ is referred to as the power spectral density of $x(t)$, and

$$\Phi_{xx}(\omega) = \int_{-\infty}^{\infty} \Phi_{xx}(\tau) e^{-j\omega\tau} d\tau \quad (5)$$

Similarly the cross power spectral density of two random signals $x(t)$ and $y(t)$ is defined as

$$\Phi_{xy}(\omega) = \int_{-\infty}^{\infty} \Phi_{xy}(\tau) e^{-j\omega\tau} d\tau \quad (6)$$

Now if $x(t)$ and $y(t)$ are the input and output of a linear system, respectively, the transfer function of that system can be obtained as

$$H(j\omega) = \frac{\Phi_{xy}(\omega)}{\Phi_{xx}(\omega)} = H(s) \Big|_{s=j\omega} \quad (7)$$

where $H(s)$ is the system transfer function in the Laplace domain.

If the input data can be described as a sum of sinusoids Eq. 7 can be simplified and the transfer function can be obtained using a Fourier Coefficient method where

$$H(j\omega) = \frac{C_y(j\omega)}{C_x(j\omega)} \quad (8)$$

where C_y and C_x represent Fourier coefficients whose real and imaginary parts are defined as

$$\text{Re}[C_y(j\omega_i)] = \frac{1}{T_i} \int_0^{T_i} y(t) \sin(\omega_i t) dt \quad (9)$$

$$\text{Imag}[C_y(j\omega_i)] = -\frac{1}{T_i} \int_0^{T_i} y(t) \cos(\omega_i t) dt \quad (10)$$

Each sine wave must have an integral number of cycles over the entire run length (no partial waves), and no sine wave can have a frequency that is an integral multiple of another frequency. The relative amplitudes are selected so that the resulting input represents an input disturbance which occurs naturally in the task. Another benefit of using fourier coefficients is the Fast Fourier Transform (FFT). The FFT takes advantage of the periodic properties of sinusoids to reduce the computation time dramatically, but requires the number of data points to be an integer power of two.

The least square error (LSE) method is the simplest approach mathematically, but computationally requires a large amount of storage space due to the matrix manipulations involved. In order to

perform a least squares identification on a single-loop pilot-vehicle system an appropriate model must be chosen. Model selection varies from the simple crossover model,

$$Y_p Y_c = \frac{K e^{-\tau s}}{s} \quad (11)$$

to higher order models like the precision model for single loop systems, (see ref. 2 pg 29)

$$Y_p = K_p e^{-j\omega\tau} \left(\frac{T_L j\omega + 1}{T_I j\omega + 1} \right) \left(\frac{T_K j\omega + 1}{T_K' j\omega + 1} \right) \left(\frac{1}{(T N_1 j\omega + 1) \left[\left(\frac{j\omega}{\omega_n} \right)^2 + \frac{2\zeta N_s}{\omega_n} j\omega + 1 \right]} \right) \quad (12)$$

Once a model has been chosen, the input and model output error are minimized using a least squares technique. After the error has been minimized the coefficients are obtained, and the closeness of fit is determined.

2.2 Least squares and sum of sines - Hess/Mnich.

The Hess/Mnich research consisted of the identification of pilot dynamics from inflight tracking data using least squares and Fourier transform analysis. The NASA Ames Dryden Flight Research Facility with NASA Langley provided data from two flight tests for evaluation of pilot characteristics. The task used for generating the data was an F-14 aircraft pursuing a T-38 target aircraft in both level flight and in a "3-G" wind up turn at a mach number of 0.55 at

an altitude of 10,000 feet with a separation distance of 800 feet. The F-14 pilot was using a gunsight reticle on a head-up display. The task of the F-14 pilot was to keep the reticle centered on the T-38 aircraft throughout the run. In addition to normal disturbances, the reticle in the F-14 was driven using a sum of sines as input so that the FFT results can be compared with the least squares results. (see ref. 6)

The least squares technique used by Hess/Mnich for analysis is implemented in a software package called Nonintrusive Parameter Identification Program (NIPIP) (ref. 7). This program uses a general model with undetermined coefficients and determines the coefficients by comparing the data to the output of the model using a multiple linear regression technique (running least squares estimation). This program is capable of identifying linear and nonlinear relations between input and output as long as the relationships are linear with respect to the unknown coefficients. NIPIP uses a time frame length, the period over which the identification is to be performed, that can be specified as any part of the time history. NIPIP also has the option of sliding the frame along through the time history, removing old data as new data is entered, which yields a moving average through the time history. The sliding time window was not required for the Hess/Mnich analysis.

The mathematical basis for the NIPIP program is a running least squares estimation technique. The coefficients of a prescribed difference equation approximating the relationship between the

input and output of a linear system are estimated. For example, consider the following difference equation

$$Y_k = a_1 Y_{k-1} + b_1 X_k + V_k \quad (13)$$

where Y_k , X_k , and V_k are the system output, input, and modeling error at the k^{th} sampling instant, respectively. Now considering a set of N measurements of the variables Y_k and X_k , one can write

$$Y = HC' + V \quad (14)$$

where

$$Y = \begin{bmatrix} Y_1 \\ Y_2 \\ \vdots \\ Y_N \end{bmatrix}$$

$$H = \begin{bmatrix} F_1 \\ F_2 \\ \vdots \\ F_N \end{bmatrix} \quad F_k = \begin{bmatrix} X_{k-1} & X_k \end{bmatrix} \quad C' = \begin{bmatrix} a_1 \\ b_1 \end{bmatrix} \quad (15)$$

$$V = \begin{bmatrix} V_1 \\ V_2 \\ \vdots \\ V_N \end{bmatrix}$$

Now C' is found by minimizing the sum of the squares of V , where,

$$V = Y - HC' \quad (16)$$

and the sum of the squares is

$$J = (Y - HC')^T(Y - HC') \quad (17)$$

Minimizing a scalar J with respect to a vector C' requires

$$\frac{\partial J}{\partial C'} = 0 \quad (18)$$

and

$$\det \left[\frac{\partial^2 J}{\partial C'^2} \right] > 0 \quad (19)$$

applying Eqs. 18 and 19 to Eq. 17 yields

$$H^T HC' = H^T Y \quad (20)$$

Solving for C' yields

$$C' = (H^T H)^{-1} H^T Y \quad (21)$$

It can be shown that

$$H^T H = \sum_{k=1}^N F_k^T F_k \quad (22)$$

and

$$H^T Y = \sum_{k=1}^N F_k^T Y_k \quad (23)$$

Then

$$C' = \left(\sum_{k=1}^N F_k^T F_k \right)^{-1} \sum_{k=1}^N F_k^T Y_k \quad (24)$$

where N is the number of data points. (see ref. 7)

In addition to using NIPIP and the FFT to analyze flight data Hess/Mnich also used a model to generate simulated data to test the two methods. Since the NIPIP program cannot identify time delays exactly, they chose their model with a second order denominator and a time delay that represents simplified human neuromuscular dynamics. The exact form of the mathematical model chosen was,

$$Y_p = \frac{2e^{-.15s}}{\left(\frac{s}{10}\right)^2 + 0.4s + 1} \quad (25)$$

However, by changing the order of the model ,time delays with integer multiples of the sampling period can be assumed and identified using a least squares technique. Then the quality of fit can be compared. This is the procedure followed in the Hess/Reedy research implemented in the Reedy subroutines.

Hess/Mnich produced good results with the simulated data. However due to a problem with the sum of sines input to the head up display the flight test results were not as well behaved as had been expected. Through averaging they were able to save the data and the results indicated that the crossover model fit the data in the area of crossover. (see ref. 6 fig. 9-12)

2.3 Description of the Reedy identification - similarity to NIPIP

The Reedy program consists of a least squares method applied to the data, either simulated or measured, where the transfer function is determined and converted from the z-domain into the w'-domain via the bilinear transform;

$$Z = \frac{1 + (T/2)w'}{1 - (T/2)w'} \quad (26)$$

where T is the sampling rate. Since the coefficients of the discrete transfer function are nearly impossible to interpret in the discrete time domain, the Bode plots are used to convert to the frequency domain where analysis can be readily accomplished. The Bode plot is made using the w'-plane transfer function as an approximation of the S-plane. This approximation is valid when , (see ref. 8 pg 196)

$$\omega \ll \frac{2}{T} = \frac{\omega_s}{\pi} \quad (28)$$

The previously described process is performed by two computer programs implemented as macros on CTRL-C, a computer-aided control system design package (ref. 9). The first macro is an identification of the coefficients of a difference equation representing the pilot model. The coefficients are determined by using a CTRL-C least squares method similar to the one described in part B of the background section. The identification macros are created by selecting a model from table 1; for example entry 3,

$$\frac{Y}{X}(z) = \frac{b_1 z^{-1}}{1 - a_1 z^{-1}} \quad (28)$$

where Y is the output, X is the input, and b_1 and a_1 are the coefficients to be identified. Next the difference equation is found;

$$Y(z) (1 - a_1 z^{-1}) = X(z) (b_1 z^{-1}) \quad (29)$$

or, in the discrete time domain

$$Y_k - a_1 Y_{k-1} = b_1 X_{k-1} \quad (30)$$

then

$$Y_k = a_1 Y_{k-1} + b_1 X_{k-1} \quad (31)$$

The set of N measurements yield eqn (14), with the desired coefficients obtained from eqn (24). After the parameters have been determined the model is simulated to obtain the model output Y'_k

which is then compared with the original output Y_k to obtain the quality of fit;

$$R^2 = 1 - \frac{\sum (Y_k - Y'_k)^2}{\sum Y_k^2} \quad (32)$$

an R^2 value of unity indicates an exact fit. This procedure is similar to the least squares portion of the NIPIP program without the sliding window. Although NIPIP would have performed the task, the least squares routines were written so that the student investigator would have a better understanding of the identification process and not simply be executing a "canned" program.

The second macro has several characteristics that must be taken into account when operated independently of the first macro. First, the numerator and denominator must be defined as Num and Den respectively before running the transformation program. Num and Den must be the same size, they must be row vectors, and then coefficients must be in descending powers of Z . If they are not the same order or contain zero coefficients, zeros must be added appropriately in order to achieve this constraint. The transformation macro operation is very simple when used in conjunction with one of the compatible least squares identification macros. The only information necessary is the sampling rate. The program will pause to display the w' -plane transfer function, and after depressing the return key the magnitude and phase Bode plots will be constructed.

Both macros are completely self contained programs and can be ran independently when necessary. Copies of these programs are in appendix III.

2.4 Example cases; Noise effects, Input Bandwidth effects, Delay Estimation techniques.

The example cases are simulations performed on the Advanced Continuous Simulation Language (ACSL) (ref. 10) to generate data for the identification process. Many examples were run to build an understanding of the identification process and gain experience with the procedures. The ACSL simulation programs were written by Ronald A. Hess, Professor of Mechanical Engineering University California at Davis. Several examples of the simulation programs are listed in appendix III.

A total of six examples were run each varying in complexity. Five test cases were run using the same system transfer function, and one higher order multi-loop example was used. This transfer function

$$\frac{100e^{-\tau_0s}}{s[s^2+4s+100]} \quad (33)$$

was chosen because it represents a second order system with an integration and a time delay and is typical of pilot-vehicle dynamics ($Y_p Y_c$) in single-loop tasks. The simulations were run with a time step of 0.05 seconds for 102.4 seconds yielding 2048 data points

(2^{11}), thereby meeting the "power of 2" requirement for FFT analysis. The FFT was used as a comparison to the least squares in some of the examples. The first five test cases run were, an open loop system with $\tau_0=0.0$ seconds (figure 1), a closed single loop system with $\tau_0=0.0$ seconds (figure 2), a closed single loop system with $\tau_0=0.0$ seconds and injected noise (figure 3), a closed single loop system with $\tau_0=0.3$ seconds and injected noise, and a closed single loop system with $\tau_0=0.0$ seconds, injected noise and a bias error (figure 4). In each of these test cases the $C(s)/E(s)$ transfer function was identified. The last example was a multi-loop hovering helicopter with a realistic pilot model with noise and a bias error (figure 5). The Q/X_e transfer function was identified in this case. The Q/X_e transfer function is a "composite", and it is similar to a transfer function to be measured in the CH-47B simulation to be discussed later. From these six examples many comparisons can be made. The effects of noise, bias, delay, cutoff frequency, and open loop versus closed loop dynamics on the quality of the identifications will be discussed presently.

An injected noise signal with a root-mean-square (RMS) value of 0.1 times the input RMS does not effect the identification to any appreciable extent. This is indicated in figure 6 and table 2. Increasing the RMS value to 1.0 times the input RMS, however, severely compromises the least- squares identification.

In table 2 and in subsequent tables listing the model used for the identification of the transfer function, the model column contains a code. The first two digits represent the entry position in

table 1, the second two digits represent the time delay in integer multiples of the sampling rate, and the last digit indicates if the routine contains a bias identification. For example, Z8D0B represents entry 8 with zero delay and a bias identification.

The effect of bias appears in figure 7 and table 3. Although not as dramatic as the noise effects, the bias error reduces the ability to identify the system correctly. In table 3 the last three rows correspond to runs in which a unity constant bias term was added to the simulation (fig. 4), and when an identification routine with a bias identification is used a definite improvement results.

The effect of delay is apparent in figure 8 and tables 4 and 5. As expected, increasing the delay decreases the correlation coefficient. It is important that the delay be correctly identified for best results. Table 5 shows that when the delay in the identification matches the delay in the system the correlation coefficient is maximized.

The effect of input cutoff frequency is shown in figure 9, 10 and 11 and in tables 2, 3, 4, and 6. Cutoff frequency appears to have no effect on the open loop and closed loop with zero noise, zero bias and zero delay examples. However, in all other test cases the increase in cutoff frequency reduced the correlation coefficient. This effect is most noticeable in the delay, noise, zero bias example, and can be seen in the last three rows of table 4. The sum of sines cutoff frequencies and their corresponding magnitudes are listed in table 7.

Identification of the open-loop transfer function in closed-loop versus open-loop operation was also undertaken and the results appear in figure 12 and 13 and in table 6. Two different inputs were utilized; the sum of sines and a unit step. The sum of sines, open-loop identification varies slightly at the high and low ends of the frequency range, but the deviation is insignificant. Identification of the open-loop transfer function in closed-loop versus open-loop operation with zero noise using both FFT and LSE techniques was undertaken. The medium cutoff sum of sines input was used.

The results appear in figures 14 and 15.

The last example was the multi-loop hovering helicopter with a realistic pilot model. Comparisons were made between the FFT, the least squares without bias, and the least squares with bias. The results show that the least squares with bias corresponds very well with the FFT, and yields a high correlation coefficient. See figures 16, 17 and table 8. The value of bias calculated by the identification subroutines cannot be compared with the bias in the single loop examples, due to the location in the model where the signals are measured.

3.0 A multi-axis manned simulation task

Data obtained from the CH-47B variable-stability helicopter at the NASA Ames Research Center was analyzed using the LSE and the FFT identification procedures outlined previously. The transfer functions identified are presented in bode form to facilitate comparison. The experimental tracking task was performed while

the helicopter was in the attitude command/attitude hold dynamic mode (ref. 11). During the precision tracking task the pilot attempts to maintain a hovering position above a pad symbol, while the pad symbol is driven by a forcing function. The forcing function is a random appearing sum of sinusoids (tables 9 and 10). The sampling interval for the simulation was 0.05 seconds. A run length of 102.4 seconds yielding 2048 (2^{11}) data points was used in order to meet the "power of 2" requirement of the FFT analysis technique.

The subjects used in this experiment were an engineer and a test pilot. Each of the two subjects performed five runs on three different configurations of a tracking task. In the first configuration the pilot controlled only the longitudinal motion of the helicopter with the aid of the complete display (figure 18). In the second configuration the subject controlled both the lateral and longitudinal motion of the helicopter with the aid of the complete display. In the final configuration the subject controlled both the lateral and longitudinal motion of the helicopter, but without the acceleration symbol on the display.

Three transfer functions were analyzed using the different configurations; these were: X/X_{pad} , X_{ball}/X_{pad} , and X_{ball}/X_{ball} error (see figure 19). The X/X_{pad} transfer function is defined between the longitudinal position of the helicopter and the longitudinal position of the hover pad, measured in feet from a fixed point on the earth. The X_{ball}/X_{pad} "composite" transfer function is defined between the position of the acceleration symbol relative to the center of the display and the position of the hover pad measured from a fixed

point on the earth, both measured in display units. The Xball/Xball error transfer function is defined between Xball and the longitudinal error between the displayed hover pad and the acceleration ball, again, both in screen units. The X/Xpad transfer function was analyzed using all three configurations, while the composite and the Xball/Xball error transfer functions were analyzed using only the first two configurations.

For the X/Xpad transfer function identifications a good correlation exists between the LSE and the FFT when the acceleration symbol is present (see figures 20 - 23), but when the acceleration symbol is removed the comparison becomes poor (see figures 24 and 25). The correlation coefficients are lower for LSE identifications without the acceleration symbol (see tables 11 - 16), and a lightly-damped mode appears in the bode plots. The mode, evident in both the FFT and the LSE plots, indicates a decrease in closed-loop system stability. Another comparison demonstrating the utility of the acceleration symbol appears in figures 26 and 27 . These two figures are plots of the actual output X, the simulated output X' for subject 1 and the command signal Xpad. The simulated output comes from the LSE program just before calculating the correlation coefficient. After the parameters or coefficients of the transfer function are identified, the program simulates the identified transfer function and compares the simulated output to the actual output. It is this simulated data that is plotted with the actual data versus time in figures 26 and 27. The correlation coefficients for figure 26 and 27 are 0.9883 and 0.7997 respectively

(see tables 13 and 15). From this analysis it is obvious that the use of the acceleration symbol greatly increases the pilots ability to maintain a hovering position over a moving object. The poor performance evident in figure 26 even with the acceleration ball is a result of the challenging nature of the sum of sines input.

Figures 28-31 show the LSE and FFT measurements for the Xball/Xball error transfer function, for each subject and configuration. Tables 21-24 show the pertinent parameters for these measurements. As the tables indicate, only the FFT measurements were reliable for this transfer function. The LSE technique yielded either unstable transfer functions (unbounded R^2 values) or very low R^2 values. This poor identification performance with the LSE technique may be do to the effects of noise injection by the subjects (remnant). Note that large noise injection did adversely effect LSE identification performance in the example case in Section 2.4.

The FFT results of figures 28-31 and tables 21-24 were quite acceptable. The data can be interpreted in terms of the crossover model of Eq. 11, with crossover frequencies on the order of 2.0 rad/sec and time delays of approximately 0.2 secs.

The composite transfer function Xball/Xpad yields important information about the assumed pilot control structure shown in figure 19. This loop structure assumes single-loop compensatory behavior on the part of the pilot, i.e. that X_e , itself, is not used by the pilot, only what has been called Xball error. Thus, although figure 19 shows two loops being closed, only the inner loop is

assumed to be closed by the pilot. Now, in order to improve tracking performance, the pilot might adopt what would be interpreted as pursuit behavior in the single loop manual control structure of figure 19 (ref. 2), or multi-loop behavior in terms of the multi-loop manual control structure of figure 32. In other words X_e might be used by the pilot and be subject to compensation. The resulting compensated signal would then be compared with X_{ball} and the difference be used to close the inner control loop. This is the multi-loop manual control structure shown in figure 32. Note that the inner loop error signal is now not X_{ball} error, but some internally generated error based upon the difference between the compensated X_e (called X_{ec} in figure 32) and X_{ball} .

Figures 33-36 show measured composite transfer functions X_{ball}/X_{pad} for the two subjects for longitudinal tracking alone and simultaneous longitudinal and lateral tracking. Now the transfer function X_{ball}/X_{pad} can be written as a product or composite of two other transfer functions as,

$$\frac{X_{ball}}{X_{pad}} = \frac{X_{ball}}{X_e} \cdot \frac{X_e}{X_{pad}} \quad (34)$$

Now, the second of these, X_e/X_{pad} , is the error-to-input transfer function for the outer loop. Figures 20-23, show the closed loop X/X_{pad} transfer functions obtained in this study. Defining bandwidth as that frequency where the phase goes through -90 degrees these figures indicate a closed loop bandwidth of

around 0.30 rad/sec. This means that the X_e/X_{pad} transfer function will be very close to unity for all frequencies much beyond 0.30 rad/sec. Thus

$$\frac{X_{ball}}{X_{pad}} = \frac{X_{ball}}{X_e} \quad (35)$$

for $\omega > 0.30$ rad/sec. But the transfer function can be obtained as

$$\frac{X_{ball}}{X_e} = \frac{X_{ball}/X_{ball \text{ error}}}{1 + X_{ball}/X_{ball \text{ error}}} \quad (36)$$

Recall that the $X_{ball}/X_{ball \text{ error}}$ transfer function has already been obtained, at least in terms of FFT measurements (see figures 28-31). Taking the FFT measurements of figure 28 as a representative sample, an acceptable fit to the data was obtained in the form of a rational transfer function. Now, forming X_{ball}/X_e using this fit, and approximating X_e/X_{pad} as

$$\frac{X_e}{X_{pad}} = \frac{s}{s + 0.3} \quad (37)$$

one obtains figure 37 from the product on the right hand side of Eq. 34. If no compensation of X_e is occurring, then figure 34 should resemble figures 33-36 in the frequency range $\omega > 0.03$ rad/sec. Looking at the amplitude ratio, this is not the case for frequencies above around 2.0 rad/sec. The measurement of figures 33-36 all indicate that the amplitude ratios are relatively flat and greater than unity in value, whereas the amplitude ratio of figure 37 has begun to fall off at around 2

rad/sec. The LSE result with the highest R^2 value (run 4, table 20) is shown for comparison. Thus, some form of pilot compensation as suggested in figure 32, is probably occurring in the outer loop to cause this discrepancy. This does not imply that the FFT measurements assuming the loop closure structure of figure 19 are incorrect, rather they reflect the effective compensatory behavior of the pilot.

Thus the FFT and least-squares measurements of the composite transfer function have led to the discovery of pursuit behavior in terms of a single-loop manual control structure as shown in figure 19, or, equivalently, multi-loop behavior, in terms of the control structure of figure 32. While the evidence for this behavior has been obtained indirectly, the data supporting it has been quite consistent. As the pertinent figures and tables for the Xball/Xpad transfer functions indicate, twice the standard deviation of the FFT data is typically less than a symbol width in magnitude, and the R^2 values for the least squares data are typically greater than 0.95.

4.0 Conclusions

- 1.) After preliminary investigation with synthetic data, Fast Fourier Transform (FFT) and Least Square Error (LSE) estimation techniques were applied to the identification of pilot-vehicle dynamics in a realistic flight simulation task.
- 2.) With the exception of the identification of the Xball to Xball error transfer function, comparisons between the FFT and LSE techniques were, in general, good. No acceptable LSE identification of the aforementioned transfer function was found. It was thought this poor LSE performance might be attributed to human noise injection in the inner control loop.
- 3.) The FFT identification of the Xball to Xball error transfer function could be described in terms of the well-known crossover model of the human pilot.
- 4.) The identification of a composite transfer function yielded some indirect evidence of pursuit tracking behavior on the part of the test subjects.

5.0 References

1. McRuer, D.T., and Krendel, E., "Dynamic Response of Human Operators," U.S. Air Force Wright Air Development Center, WADC-TR-56-524, Oct. 1957.
2. McRuer, D.T., Krendel, E., "Mathematical Models of Human Pilot Behavior," AGARDograph, number 188, 1974.
3. McRuer, D.T., "Human Dynamics in Man-Machine Systems," Automatica, volume 16, number 3, pages 237-253, 1980.
4. Hess, R.A., "A Structural Model of the Adaptive Human Pilot," Journal of Guidance and Control, Vol. 2, No. 3, pages 221-227, May-June 1979.
5. Wingrove, R. C. "Comparison of Methods for Identifying Pilot Describing Functions from Closed-Loop Operating Records," Ames Research Center, NASA TN D-6235, 1971.
6. Hess, R.A., and Mnich, M.A., "Identification of Pilot Dynamics from In-Flight Tracking Data," Journal of Guidance, Control, and Dynamics, Vol. 9, No. 4, pp. 433-440, July-August 1986.
7. Hanson, G. D. and Jewell, W. F., "Non-Intrusive Parameter Identification Procedure Users Guide," NASA CR-170398 April 1983.
8. Phillips, C. L. and Nagle, H. T., Jr., "Digital Control Systems Analysis and Design," Prentice Hall.
9. Anon., "CTRL-C, A Language for the Computer-Aided Design of Multivariable Control Systems," Systems Control Technology 1983.
10. Anon., "ACSL, Advanced Continuous Simulation Language," Mitchell and Gauthier, Assoc., 1984.

11. Eshow, M. , Aiken, E., and Hindson, W. "Preliminary Results of a Flight Investigation of Rotorcraft Control and Display Laws for Hover," American Helicopter Soc. Mideast Region National Specialists Meeting in Rotorcraft Flight Controls and Avionics, Cherry Hill, NJ. Oct. 13-15, 1987.

6.0 Appendix I Tables

TABLE 1

Entry No.	z-Transform	No. of Unknowns	Physical System
1	$b_1 z^{-1}$	1	K (pure gain)
2	$\frac{b_1 T z^{-1}}{1 - z^{-1}}$	1	$\frac{K}{s}$ (integrator)
3	$\frac{b_1 z^{-1}}{1 - a_1 z^{-1}}$	2	$\frac{Ka}{s+a}$ (1st-order lag)
4	$\frac{b_1 z^{-1} + b_2 z^{-2}}{1 - a_1 z^{-1} - a_2 z^{-2}}$	4	$\frac{K\omega^2}{[\zeta; \omega]}$
5	$\frac{b_1 z^{-1} + b_2 z^{-2}}{1 - a_1 z^{-1} - a_2 z^{-2}} (z^{-P})$	4	$\frac{K(s+a)}{[\zeta; \omega]} e^{-ps}$
6	$\frac{b_1 z^{-1} + b_2 z^{-2}}{1 - a_1 z^{-1}} (z^{-P})$	3	$\frac{K(s+a)}{(s+b)} e^{-ps}$
7	$\frac{b_1 z^{-1} + b_2 z^{-2}}{1 - a_1 z^{-1} - a_2 z^{-2}}$	4	$\frac{K(s+a)}{s(s+b)}$
8	$\frac{b_1 z^{-1} + b_2 z^{-2} + b_3 z^{-3}}{1 - a_1 z^{-1} - a_2 z^{-2} - a_3 z^{-3}}$	6	$\frac{K(s+a)}{(s+b) [\zeta; \omega]}$
9	$\frac{b_1 z^{-1} + b_2 z^{-2} + b_3 z^{-3} + b_4 z^{-4}}{1 - a_1 z^{-1} - a_2 z^{-2} - a_3 z^{-3}}$	7	$\frac{K[\zeta_n; \omega_n]}{[\zeta_1; \omega_1][\zeta_2; \omega_2]}$

TABLE 2 - NOISE AND CUTOFF FREQUENCY COMPARISON

INPUT	R ²	NOISE	ACTUAL DELAY	IDENTIFIED BIAS	LOOP STRUCTURE	MODEL
Σ SINES MED CUT	0.9997	0.0	0.0	N.I.	CLOSED	Z8D0
Σ SINES LOW CUT	0.9940	0.1	0.0	N.I.	CLOSED	Z8D2
Σ SINES MED CUT	0.9809	0.1	0.0	N.I.	CLOSED	Z8D2
Σ SINES HIGH CUT	0.9552	0.1	0.0	N.I.	CLOSED	Z8D2
Σ SINES MED CUT	0.1114	1.0	0.0	N.I.	CLOSED	Z8D4

* N.I. - NOT IDENTIFIED

TABLE 3 - BIAS COMPARISON

INPUT	R ²	NOISE	ACTUAL DELAY	IDENTIFIED BIAS	LOOP STRUCTURE	MODEL
Σ SINES LOW CUT	0.9802	0.1	0.3	N.I.	CLOSED	Z8D4
Σ SINES MED CUT	0.8916	0.1	0.3	N.I.	CLOSED	Z8D4
Σ SINES HIGH CUT	0.7276	0.1	0.3	N.I.	CLOSED	Z8D5
Σ SINES LOW CUT	0.9969	0.1	0.3	0.9961	CLOSED	Z8D3B
Σ SINES MED CUT	0.9904	0.1	0.3	0.9911	CLOSED	Z8D3B
Σ SINES HIGH CUT	0.9839	0.1	0.3	0.9954	CLOSED	Z8D4B

* N.I. - NOT IDENTIFIED

TABLE 4 - DELAY COMPARISON

INPUT	R ²	NOISE	ACTUAL DELAY	IDENTIFIED BIAS	LOOP STRUCTURE	MODEL
Σ SINES LOW CUT	0.9940	0.1	0.0	N.I.	CLOSED	Z8D2
Σ SINES MED CUT	0.9809	0.1	0.0	N.I.	CLOSED	Z8D2
Σ SINES HIGH CUT	0.9552	0.1	0.0	N.I.	CLOSED	Z8D2
Σ SINES LOW CUT	0.9802	0.1	0.3	N.I.	CLOSED	Z8D4
Σ SINES MED CUT	0.8916	0.1	0.3	N.I.	CLOSED	Z8D4
Σ SINES HIGH CUT	0.7276	0.1	0.3	N.I.	CLOSED	Z8D5

* N.I. - NOT IDENTIFIED

TABLE 5 - IDENTIFIED DELAY COMPARISON

INPUT	R ²	NOISE	ACTUAL DELAY	IDENTIFIED BIAS	LOOP STRUCTURE	MODEL
Σ SINES MED CUT	0.9338	0.1	0.0	N.I.	CLOSED	Z8D0
Σ SINES MED CUT	0.9540	0.1	0.0	N.I.	CLOSED	Z8D1
Σ SINES MED CUT	0.9809	0.1	0.0	N.I.	CLOSED	Z8D2
Σ SINES MED CUT	0.9555	0.1	0.0	N.I.	CLOSED	Z8D3
Σ SINES MED CUT	UNSTABLE	0.1	0.0	N.I.	CLOSED	Z8D4
Σ SINES MED CUT	UNSTABLE	0.1	0.0	N.I.	CLOSED	Z8D5
Σ SINES MED CUT	UNSTABLE	0.1	0.0	N.I.	CLOSED	Z8D6

* N.I. - NOT IDENTIFIED

TABLE 6 - OPEN VS. CLOSED LOOP

INPUT	R ²	NOISE	ACTUAL IDENTIFIED LOOP			MODEL
			DELAY	BIAS	STRUCTURE	
\sum SINES LOW CUT	1.0	0.0	0.0	N.I.	OPEN	Z8D0
\sum SINES MED CUT	1.0	0.0	0.0	N.I.	OPEN	Z8D0
\sum SINES HIGH CUT	1.0	0.0	0.0	N.I.	OPEN	Z8D0
\sum SINES LOW CUT	0.9998	0.0	0.0	N.I.	CLOSED	Z8D0
\sum SINES MED CUT	0.9997	0.0	0.0	N.I.	CLOSED	Z8D0
\sum SINES HIGH CUT	0.9998	0.0	0.0	N.I.	CLOSED	Z8D0
STEP	1.0	0.0	0.0	N.I.	OPEN	Z8D0
STEP	0.9999	0.0	0.0	N.I.	CLOSED	Z8D0

* N.I. - NOT IDENTIFIED

TABLE 7 - \sum SINES

$$r(t) = A_0 \sum_{i=1}^{12} A_i \sin(\omega_i t)$$

i	ω_i (rad/sec)	LOW CUTOFF	MED CUTOFF	HIGH CUTOFF	HELICOPTER
		$A_0=1/1.546$ A_i	$A_0=1/3.03$ A_i	$A_0=1/4.02$ A_i	$A_0=1$ A_i
1	0.1841	1	1	1	17.6
2	0.3068	1	1	1	17.6
3	0.4909	1	1	1	17.6
4	0.7977	0.1	1	1	17.6
5	1.1660	0.1	1	1	1.76
6	1.7790	0.1	1	1	1.76
7	2.8230	0.1	0.1	1	1.76
8	4.6630	0.1	0.1	1	0.88
9	6.9330	0.1	0.1	0.1	0.88
10	8.9580	0.1	0.1	0.1	0
11	12.0880	0.1	0.1	0.1	0
12	17.9780	0.1	0.1	0.1	0

TABLE 8 - MULTI-LOOP HELICOPTER COPARISON

INPUT	R ²	NOISE	ACTUAL DELAY	IDENTIFIED BIAS	LOOP STRUCTURE	MODEL
Σ SINES	0.9644	0.0	0.0	N.I.	MULTI	Z9D0
Σ SINES	0.9664	0.0	0.0	-14.01	MULTI	Z9D0B
Σ SINES	0.9573	0.1	0.0	N.I.	MULTI	Z9D0
Σ SINES	0.9578	0.1	0.0	-13.95	MULTI	Z9D0B

* N.I. - NOT IDENTIFIED

TABLE 9 - \sum SINES FOR THE LONGITUDINAL DIRECTION OF THE CH-47B HELICOPTER.

$$r(t) = A_0 \sum_{i=1}^{12} A_i \sin(\omega_i t)$$

i	ω_i (rad/sec)	AMPLITUDE	NO. OF CYCLES
1	0.1841	17.6	3
2	0.3068	17.6	5
3	0.4909	17.6	8
4	0.7977	17.6	13
5	1.1660	1.76	19
6	1.7790	1.76	29
7	2.8230	1.76	46
8	4.6630	0.88	76
9	6.9330	0.88	113

TABLE 10 - \sum SINES FOR THE LATERAL DIRECTION OF THE CH-47B HELICOPTER.

$$r(t) = A_0 \sum_{i=1}^{12} A_i \sin(\omega_i t)$$

i	ω_i (rad/sec)	AMPLITUDE	NO. OF CYCLES
1	0.2454	17.6	4
2	0.4295	17.6	7
3	0.6750	17.6	11
4	0.9204	17.6	15
5	1.4110	1.76	23
6	2.2700	1.76	37
7	3.7430	1.76	61
8	5.7060	0.88	93
9	7.7930	0.88	127

FREQUENCY (RAD/SEC)	ω_1	ω_2	ω_3	ω_4	ω_5	ω_6	ω_7	ω_8	ω_9
$\nu + \sigma$	0.1841	0.3068	0.4909	0.7977	1.166	1.779	2.823	4.663	6.934
MAGNITUDE	0.85	0.72	0.63	0.53	0.29	0.077	0.017	0.0063	0.0055
ν	0.83	0.70	0.61	0.51	0.24	0.072	0.013	0.0040	0.0029
$\nu - \sigma$	0.81	0.67	0.60	0.50	0.19	0.066	0.010	0.0026	0.0015
PHASE	-48	-71	-101	-158	-228	-302	-380	-524	-832
σ	1	2	2	1	14	18	18	26	42

Fast fourier transform results for the X/Xpad transfer function for subject 1, longitudinal tracking only.

$\sum R^2$	IDENTIFIED BIAS	IDENTIFIED DELAY	COEFFICIENTS OF THE IDENTIFIED TRANSFER FUNCTION IN THE Z-DOMAIN IN DESCENDING ORDER NUMERATOR FIRST
1 0.9152	-3.4010	Z^{-10}	2.8007, -2.6124, 0.8115; 0.0088, -0.0187, 0.0100
2 0.7262	-3.7675	Z^{-3}	2.3861, -1.7956, 0.4091; 0.0124, -0.0234, 0.0114
3 0.9832	-0.0823	Z^{-1}	2.9657, -2.9334, 0.9677; 0.0004, -0.0009, 0.0005
4 NO DATA			
5 0.9764	0.5552	Z^{-1}	2.9609, -2.9240, 0.9631; 0.0005, -0.0010, 0.0005

Least squares results for the X/Xpad transfer function for subject 1, longitudinal tracking only.

TABLE 11

FREQUENCY (RAD/SEC)	ω_1	ω_2	ω_3	ω_4	ω_5	ω_6	ω_7	ω_8	ω_9
MAGNITUDE	$\nu + \sigma$	0.3068	0.4909	0.7977	1.166	1.779	2.823	4.663	6.934
	ν	0.70	0.58	0.52	0.41	0.15	0.03	0.03	0.02
	$\nu - \sigma$	0.69	0.57	0.51	0.37	0.09	0.02	0.016	0.01
PHASE	ν	0.68	0.56	0.49	0.33	0.06	0.01	0.009	0.005
	ν	-69	-95	-144	-203	-276	-364	-563	-735
	σ	3	2	3	12	20	53	89	137

Fast fourier transform results for the X/Xpad transfer function for subject 2, longitudinal tracking only.

$\sum R^2$	IDENTIFIED BIAS	IDENTIFIED DELAY	COEFFICIENTS OF THE IDENTIFIED TRANSFER FUNCTION IN THE Z-DOMAIN IN DESCENDING ORDER NUMERATOR FIRST
1 0.9789	-0.6211	Z^0	2.9667, -2.9356, 0.9689, 0.0005, -0.0009, 0.0005
2 0.9843	-0.9776	Z^0	2.9645, -2.9314, 0.9669, 0.0004, -0.0010, 0.0005
3 0.9385	-0.6012	Z^0	2.9631, -2.9287, 0.9656, 0.0005, -0.0010, 0.0006
4 0.9779	-0.0346	Z^{-1}	2.9636, -2.9295, 0.9659, 0.0004, -0.0010, 0.0006
5 0.9711	-0.2645	Z^{-1}	2.9609, -2.9244, 0.9635, 0.0006, -0.0012, 0.0007

Least squares results for the X/Xpad transfer function for subject 2, longitudinal tracking only.

TABLE 12

FREQUENCY (RAD/SEC)	ω_1	ω_2	ω_3	ω_4	ω_5	ω_6	ω_7	ω_8	ω_9
	$\nu + \sigma$	0.1841	0.3068	0.4909	0.7977	1.166	1.779	2.823	4.663
MAGNITUDE	0.83	0.70	0.59	0.48	0.31	0.10	0.018	0.004	0.0028
ν	0.82	0.68	0.58	0.47	0.25	0.08	0.016	0.003	0.0015
$\nu - \sigma$	0.81	0.67	0.57	0.46	0.20	0.07	0.014	0.002	0.0008
PHASE	-48	-71	-97	-145	-214	-296	-373	-487	-657
σ	1	1	1	2	10	7	17	72	61

FFT results for the X/Xpad transfer function, subject 1, lateral and longitudinal tracking.

Z^2	IDENTIFIED BIAS	IDENTIFIED DELAY	COEFFICIENTS OF THE IDENTIFIED TRANSFER FUNCTION IN THE Z-DOMAIN IN DESCENDING ORDER NUMERATOR FIRST
1	-0.4900	Z^0	2.9627, -2.9279, 0.9651; 0.0004, -0.0008, 0.0005
2	-0.5622	Z^0	2.9615, -2.9253, 0.9638; 0.0004, -0.0009, 0.0005
3	0.0002	Z^0	2.9609, -2.9243, 0.9634; 0.0004, -0.0009, 0.0005
4	-0.1742	Z^{-1}	2.9640, -2.9305, 0.9664; 0.0004, -0.0008, 0.0005
5	0.5565	Z^{-1}	2.9599, -2.9223, 0.9624; 0.0004, -0.0009, 0.0005

LSE results for the X/Xpad transfer function, subject 1, lateral and longitudinal tracking.

TABLE 13

FREQUENCY (RAD/SEC)	ω_1	ω_2	ω_3	ω_4	ω_5	ω_6	ω_7	ω_8	ω_9
$\nu + \sigma$	0.1841	0.3068	0.4909	0.7977	1.166	1.779	2.823	4.663	6.934
MAGNITUDE	0.83	0.71	0.56	0.47	0.35	0.11	0.039	0.020	0.013
ν	0.81	0.69	0.55	0.46	0.28	0.10	0.025	0.007	0.005
$\nu - \sigma$	0.78	0.67	0.54	0.45	0.23	0.09	0.016	0.003	0.002
PHASE	-45	-69	-95	-142	-201	-279	-368	-441	-617
σ	2	1	1	2	15	10	12	111	120

FFT results for the X/Xpad transfer function, subject 2, lateral and longitudinal tracking.

Z	R^2	IDENTIFIED BIAS	IDENTIFIED DELAY	COEFFICIENTS OF THE IDENTIFIED TRANSFER FUNCTION IN THE Z-DOMAIN IN DESCENDING ORDER NUMERATOR FIRST
1	0.9628	-0.6071	Z^{-5}	1.5180, -0.0965, -0.4226; 0.0056, -0.0166, -0.0118
2	0.9860	-0.8693	Z^{-1}	2.9559, -2.9147, 0.9587; 0.0004, -0.0010, 0.0006
3	0.9687	-0.4745	Z^0	2.9602, -2.9231, 0.9628; 0.0005, -0.0010, 0.0006
4	0.9887	-0.5715	Z^{-1}	2.9572, -2.9172, 0.9599; 0.0006, -0.0012, 0.0007
5	0.9854	-0.0356	Z^0	2.9613, -2.9252, 0.9639; 0.0004, -0.0009, 0.0005

LSE results for the X/Xpad transfer function, subject 2, lateral and longitudinal tracking.

TABLE 14

FREQUENCY (RAD/SEC)	ω_1	ω_2	ω_3	ω_4	ω_5	ω_6	ω_7	ω_8	ω_9
$\nu + \sigma$	0.1841	0.3068	0.4909	0.7977	1.166	1.779	2.823	4.663	6.934
MAGNITUDE	1.46	1.43	0.66	0.44	2.27	0.29	0.10	0.12	0.09
ν	1.08	0.83	0.54	0.36	1.31	0.25	0.07	0.06	0.04
$\nu - \sigma$	0.79	0.48	0.44	0.29	0.76	0.22	0.06	0.04	0.02
PHASE	-93	-118	-100	-134	-163	-353	-434	-640	-939
σ	68	67	34	14	64	40	50	109	143

FFT results for the X/Xpad transfer function, subject 1, lateral and longitudinal tracking, no acceleration ball.

\bar{z}	R^2	IDENTIFIED BIAS	IDENTIFIED DELAY	COEFFICIENTS OF THE IDENTIFIED TRANSFER FUNCTION IN THE Z-DOMAIN IN DESCENDING ORDER NUMERATOR FIRST
1	UNSTABLE			
2	0.6168	-1.6299	z^0	2.9904, -2.9837, 0.9934; 0.0007, -0.0015, 0.0008
3	UNSTABLE			
4	0.3731	0.5432	\bar{z}^8	2.9952, -2.9930, 0.9979; 0.0003, -0.0007, 0.0004
5	0.7997	-0.8485	\bar{z}^2	2.9894, -2.9812, 0.9918; 0.0007, -0.0015, 0.0008

LSE results for the X/Xpad transfer function, subject 1, lateral and longitudinal tracking, no acceleration ball.

TABLE 15

FREQUENCY (RAD/SEC)	ω_1	ω_2	ω_3	ω_4	ω_5	ω_6	ω_7	ω_8	ω_9
$\nu + \sigma$	0.1841	0.3068	0.4909	0.7977	1.166	1.779	2.823	4.663	6.934
MAGNITUDE									
ν	1.50	1.42	0.62	0.34	1.07	0.66	0.12	0.16	0.11
$\nu - \sigma$	0.84	0.85	0.41	0.26	0.61	0.41	0.08	0.06	0.03
PHASE									
ν	0.47	0.52	0.27	0.20	0.35	0.26	0.05	0.02	0.01
ν	-68	-75	-116	-110	-91	-175	-510	-461	-522
σ	31	27	58	15	57	98	110	71	70

FFT results for the X/Xpad transfer function, subject 2, lateral and longitudinal tracking, no acceleration ball.

Z	R^2	IDENTIFIED BIAS	IDENTIFIED DELAY	COEFFICIENTS OF THE IDENTIFIED TRANSFER FUNCTION IN THE Z-DOMAIN IN DESCENDING ORDER NUMERATOR FIRST
1	0.0898	-0.7542	z^{-12}	2.9957, -2.9936, 0.9979; 0.0012, -0.0027, 0.0015
2	UNSTABLE			
3	0.4199	-0.1960	z^0	2.9888, -2.9815, 0.9927; 0.0003, -0.0007, 0.0004
4	0.4166	-0.6512	z^0	2.9912, -2.9857, 0.9945; -0.0001, 0.0003, -0.0001
5	0.8008	-5.4214	z^0	2.9889, -2.9826, 0.9937; 0.0006, -0.0012, 0.0006

LSE results for the X/Xpad transfer function, subject 2, lateral and longitudinal tracking, no acceleration ball.

TABLE 16

FREQUENCY (RAD/SEC)	ω_1	ω_2	ω_3	ω_4	ω_5	ω_6	ω_7	ω_8	ω_9
	$\nu + \sigma$	0.1841	0.3068	0.4909	0.7977	1.166	1.779	2.823	4.663
MAGNITUDE	0.76	1.05	1.39	1.85	1.63	1.06	0.90	1.19	1.17
	0.75	1.01	1.36	1.79	1.35	1.04	0.72	1.00	1.10
$\nu - \sigma$	0.74	0.98	1.34	1.74	1.11	1.02	0.57	0.84	1.04
PHASE	53	38	21	-7	-40	-62	-80	-125	-157
	2	2	2	1	13	15	14	9	5

FFT results for the "composite" transfer function, subject 1, longitudinal tracking only.

$\sum R^2$	IDENTIFIED BIAS	IDENTIFIED DELAY	COEFFICIENTS OF THE IDENTIFIED TRANSFER FUNCTION IN THE Z-DOMAIN IN DESCENDING ORDER NUMERATOR FIRST
1 0.8903	1.6789	Z^{-4}	1.8964, -1.3197, 0.4186; -1.0291, 2.8095, -1.7810
2 0.9088	-0.1150	Z^{-4}	1.8705, -1.3720, 0.4958; -1.1056, 3.0899, -1.9853
3 0.9201	0.3488	Z^{-3}	2.0035, -1.3447, 0.3376; -0.8380, 2.1467, -1.3088
4 NO	DATA		
5 0.9441	0.6570	Z^{-2}	1.9791, -1.2565, 0.2743; -0.7672, 1.9427, -1.1758

LSE results for the "composite" transfer function, subject 1, longitudinal tracking only.

TABLE 17

FREQUENCY (RAD/SEC)	ω_1	ω_2	ω_3	ω_4	ω_5	ω_6	ω_7	ω_8	ω_9
$\nu + \sigma$	0.1841	0.3068	0.4909	0.7977	1.166	1.779	2.823	4.663	6.934
MAGNITUDE	0.87	1.02	1.29	1.81	2.11	1.85	1.32	1.20	1.63
ν	0.67	1.01	1.27	1.77	1.94	1.52	1.16	1.14	1.44
$\nu - \sigma$	0.52	1.00	1.25	1.73	1.77	1.25	1.03	1.09	1.27
PHASE	55	40	28	6	-18	-45	-76	-115	-165
σ	3	3	3	3	12	15	9	10	8

FFT results for the "composite" transfer function, subject 2, longitudinal tracking only.

Z^2	IDENTIFIED BIAS	IDENTIFIED DELAY	COEFFICIENTS OF THE IDENTIFIED TRANSFER FUNCTION IN THE Z-DOMAIN IN DESCENDING ORDER NUMERATOR FIRST
1	-2.3782	Z^{-3}	2.0041, -1.3142, 0.3042; -1.0372, 2.5484, -1.5114
2	-0.0447	Z^{-2}	2.0244, -1.3132, 0.2843; -0.7597, 1.9152, -1.1550
3	-0.6731	Z^{-3}	1.9039, -1.1283, 0.2187; -0.9311, 2.3434, -1.4120
4	-3.8347	Z^{-2}	2.0462, -1.3435, 0.2938; -0.7977, 1.9397, -1.1422
5	0.0380	Z^{-2}	2.0013, -1.2800, 0.2737; -0.8889, 2.2028, -1.3133

LSE results for the "composite" transfer function, subject 2, longitudinal tracking only.

TABLE 18

FREQUENCY (RAD/SEC)	ω_1	ω_2	ω_3	ω_4	ω_5	ω_6	ω_7	ω_8	ω_9
	0.1841	0.3068	0.4909	0.7977	1.166	1.779	2.823	4.663	6.934
$\nu + \sigma$	0.74	1.02	1.30	1.69	1.86	1.49	1.17	1.09	1.44
ν	0.73	1.00	1.29	1.66	1.53	1.27	1.05	0.96	1.25
$\nu - \sigma$	0.72	0.98	1.27	1.63	1.26	1.09	0.94	0.84	1.08
ν	52	38	24	5	-27	-53	-78	-115	-177
σ	2	1	1	1	10	8	4	16	22

FFT results for the "composite" transfer function, subject 1, lateral and longitudinal tracking.

Z^2	IDENTIFIED BIAS	IDENTIFIED DELAY	COEFFICIENTS OF THE IDENTIFIED TRANSFER FUNCTION IN THE Z-DOMAIN IN DESCENDING ORDER NUMERATOR FIRST
1 0.9384	1.5854	Z^{-1}	1.9630, -1.2650, 0.2973; -1.2838, 3.0089, -1.7253
2 0.9539	0.0804	Z^{-2}	1.9553, -1.2492, 0.2890; -1.0113, 2.4877, -1.4762
3 0.9560	-1.3567	Z^{-2}	1.8825, -1.1666, 0.2785; -1.1338, 2.8104, -1.6769
4 0.9444	0.0504	Z^{-3}	1.8737, -1.2096, 0.3299; -0.8742, 2.3717, -1.4979
5 0.9510	0.7394	Z^{-4}	1.9513, -1.2439, 0.2869; -0.5509, 1.6103, -1.0591

LSE results for the "composite" transfer function, subject 1, lateral and longitudinal tracking.

TABLE 19

FREQUENCY (RAD/SEC)	ω_1	ω_2	ω_3	ω_4	ω_5	ω_6	ω_7	ω_8	ω_9
$\nu + \sigma$	0.1841	0.3068	0.4909	0.7977	1.166	1.779	2.823	4.663	6.934
MAGNITUDE									
ν	0.76	1.04	1.26	1.68	2.05	1.51	1.49	1.29	1.58
$\nu - \sigma$	0.71	1.01	1.23	1.59	1.47	1.24	1.34	1.23	1.44
PHASE									
ν	0.68	0.98	1.21	1.50	1.05	0.82	1.21	1.17	1.31
ν	54	40	28	8	-23	-45	-78	-112	-155
σ	4	2	1	2	25	7	3	9	7

FFT results for the "composite" transfer function, subject 2, lateral and longitudinal tracking.

$\sum R^2$	IDENTIFIED BIAS	IDENTIFIED DELAY	COEFFICIENTS OF THE IDENTIFIED TRANSFER FUNCTION IN THE Z-DOMAIN IN DESCENDING ORDER NUMERATOR FIRST
1 0.9601	0.1989	z^{-2}	1.8477, -0.9839, 0.1307; -0.5661, 1.5712, -1.0041
2 0.9650	-0.3476	z^{-2}	1.8432, -1.0322, 0.1822; -1.2170, 2.9331, -1.7153
3 0.8363	-2.1982	z^{-2}	1.8112, -0.9123, 0.0967; -1.0209, 2.4035, -1.3835
4 0.9671	-0.2163	z^{-1}	1.9136, -1.0837, 0.1649; -0.9789, 2.3354, -1.3561
5 0.9583	0.1806	z^{-2}	1.8552, -0.9841, 0.1232; -0.9226, 2.2518, -1.3281

LSE results for the "composite" transfer function, subject 2, lateral and longitudinal tracking.

TABLE 20

FREQUENCY (RAD/SEC)	ω_1	ω_2	ω_3	ω_4	ω_5	ω_6	ω_7	ω_8	ω_9
$\nu + \sigma$	0.1841	0.3068	0.4909	0.7977	1.166	1.779	2.823	4.663	6.934
MAGNITUDE	27.49	35.65	8.01	3.72	2.63	1.39	0.77	0.64	0.54
ν	18.94	20.36	7.40	3.45	1.92	1.10	0.65	0.57	0.53
$\nu - \sigma$	13.05	11.62	6.83	3.20	1.39	0.88	0.54	0.51	0.52
PHASE	-346	-153	-126	-133	-123	-124	-120	-154	-169
σ	105	103	12	2	13	8	15	5	4

FFT results for the Xball/Xball error transfer function, subject 1, longitudinal tracking only.

$\sum_{i=1}^n R^2$	IDENTIFIED BIAS	IDENTIFIED DELAY	COEFFICIENTS OF THE IDENTIFIED TRANSFER FUNCTION IN THE Z-DOMAIN IN DESCENDING ORDER NUMERATOR FIRST
1 UNSTABLE			
2 UNSTABLE			
3 0.1327	-0.0145	Z^{-15}	2.0645, -1.4013, 0.3364; -0.0080, 0.0146, 0.0206
4 NO DATA			
5 UNSTABLE			

LSE results for the Xball/Xball error transfer function, subject 1, longitudinal tracking only.

TABLE 21

FREQUENCY (RAD/SEC)	ω_1	ω_2	ω_3	ω_4	ω_5	ω_6	ω_7	ω_8	ω_9
$\nu + \sigma$	0.1841	0.3068	0.4909	0.7977	1.166	1.779	2.823	4.663	6.934
MAGNITUDE									
ν	68.00	36.40	20.50	5.20	3.00	1.90	0.96	0.67	0.63
$\nu - \sigma$	26.00	23.50	14.90	4.80	2.70	1.50	0.88	0.63	0.60
PHASE									
ν	10.40	15.20	10.80	4.40	2.30	1.20	0.81	0.60	0.57
σ	-119	-146	-172	-156	-173	-141	-134	-150	-174
	93	48	22	8	28	16	7	5	3

FFT results for the Xball/Xballerror transfer function, subject 2, longitudinal tracking only.

Z^2	R^2	IDENTIFIED BIAS	IDENTIFIED DELAY	COEFFICIENTS OF THE IDENTIFIED TRANSFER FUNCTION IN THE Z-DOMAIN IN DESCENDING ORDER NUMERATOR FIRST
1	0.0974	-0.1641	Z^{-10}	2.1314, -1.4086, 0.2766; 0.0131, -0.0624, 0.0547
2	0.1824	-0.3485	Z^{-10}	2.1242, -1.3939, 0.2695; -0.0237, 0.0176, 0.0186
3	0.2157	-0.2263	Z^{-10}	2.0505, -1.2409, 0.1897; -0.0088, -0.0206, 0.0388
4	UNSTABLE			
5	0.2347	-0.0662	Z^{-10}	2.1354, -1.4077, 0.2719; -0.0240, 0.0229, 0.0130

LSE results for the Xball/Xballerror transfer function, subject 2, longitudinal tracking only.

TABLE 22

FREQUENCY (RAD/SEC)	ω_1	ω_2	ω_3	ω_4	ω_5	ω_6	ω_7	ω_8	ω_9
	0.1841	0.3068	0.4909	0.7977	1.166	1.779	2.823	4.663	6.934
$\nu + \sigma$	62.75	89.13	14.07	5.82	3.58	1.54	0.89	0.66	0.60
MAGNITUDE	30.46	42.37	12.24	5.61	2.65	1.32	0.82	0.58	0.56
$\nu - \sigma$	14.78	20.14	10.65	5.42	1.95	1.13	0.75	0.51	0.53
PHASE	-1	-71	-139	-150	-130	-131	-131	-147	-170
σ	60	41	6	4	22	8	3	7	3

FFT results for the Xball/Xball error transfer function, subject 1, lateral and longitudinal tracking.

Z	R^2	IDENTIFIED BIAS	IDENTIFIED DELAY	COEFFICIENTS OF THE IDENTIFIED TRANSFER FUNCTION IN THE Z-DOMAIN IN DESCENDING ORDER NUMERATOR FIRST
1	0.0533	-0.1734	$z^{-1}3$	2.0459, -1.3260, 0.2797; 0.0418, -0.1250, 0.1063
2	0.1553	-0.1859	$z^{-1}4$	2.0407, -1.2982, 0.2566; -0.0346, 0.0238, 0.0338
3	0.0498	0.0215	$z^{-1}4$	1.9782, -1.2133, 0.2347; -0.0642, 0.0978, -0.0081
4	0.3166	-0.0582	$z^{-1}4$	1.9822, -1.2517, 0.2691; -0.0132, 0.0062, 0.0377
5	UNSTABLE			

LSE results for the Xball/Xball error transfer function, subject 1, lateral and longitudinal tracking.

TABLE 23

FREQUENCY (RAD/SEC)	ω_1	ω_2	ω_3	ω_4	ω_5	ω_6	ω_7	ω_8	ω_9
	0.1841	0.3068	0.4909	0.7977	1.166	1.779	2.823	4.663	6.934
MAGNITUDE									
$\nu + \sigma$	18.00	34.40	35.90	7.40	6.90	1.90	0.96	0.71	0.63
ν	13.60	23.90	22.80	6.50	3.90	1.60	0.91	0.66	0.61
$\nu - \sigma$	10.20	16.70	14.50	5.70	2.20	1.10	0.86	0.62	0.59
PHASE									
ν	-248	-173	-184	-162	-184	-140	-140	-149	-169
σ	54	65	12	6	47	5	6	5	3

FFT results for the Xball/Xball error transfer function, subject 2, lateral and longitudinal tracking.

Z	R^2	IDENTIFIED BIAS	IDENTIFIED DELAY	COEFFICIENTS OF THE IDENTIFIED TRANSFER FUNCTION IN THE Z-DOMAIN IN DESCENDING ORDER NUMERATOR FIRST
1	0.4116	-0.1043	z^{-14}	1.9454, -1.0607, 0.1149; 0.0080, -0.0606, 0.0707
2	0.1329	-0.2421	z^{-13}	1.9733, -1.1135, 0.1389; -0.0362, 0.0112, 0.0358
3	UNSTABLE			
4	0.0361	-0.1509	z^{-13}	2.0283, -1.1853, 0.1563; -0.0197, 0.0047, 0.0248
5	0.1144	-0.0071	z^{-11}	1.9903, -1.1000, 0.1086; 0.0304, -0.0933, 0.0699

LSE results for the Xball/Xball error transfer function, subject 2, lateral and longitudinal tracking.

TABLE 24

7.0 Appendix II Figures

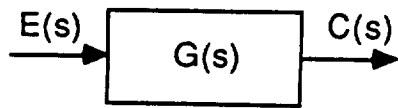


FIGURE 1 - OPEN LOOP

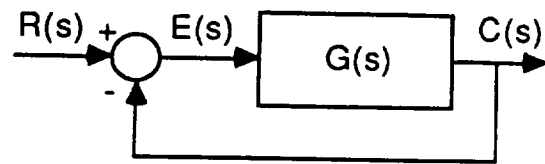


FIGURE 2 - CLOSED LOOP

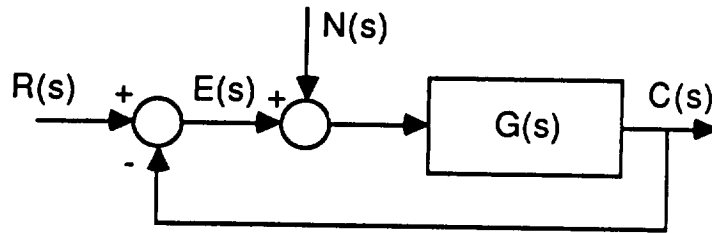
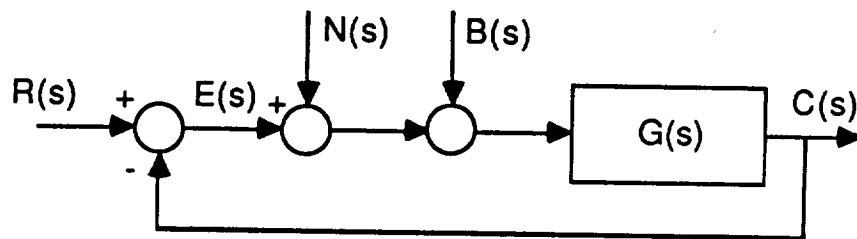
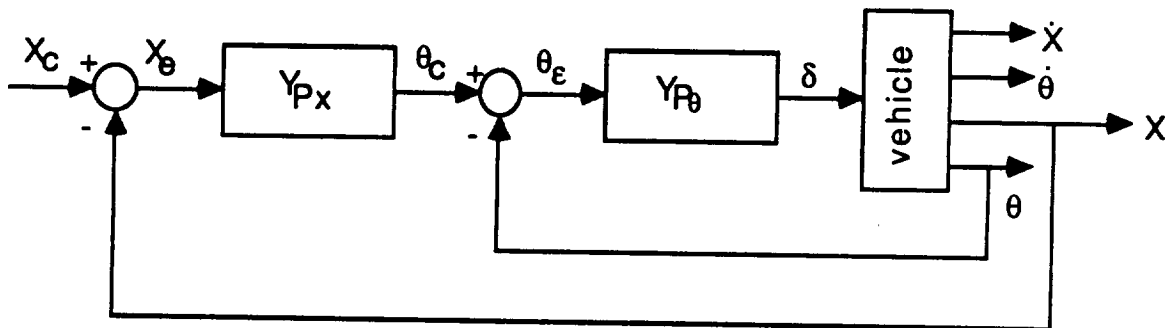
FIGURE 3 - CLOSED LOOP WITH NOISE $N(s)$ FIGURE 4 - CLOSED LOOP WITH NOISE $N(s)$ AND BIAS $B(s)$ 

FIGURE 5 - MULTI-LOOP HOVERING HELICOPTER MODEL

FIGURE 6 NOISE COMPARISON, MEDIUM CUTOFF FREQUENCY

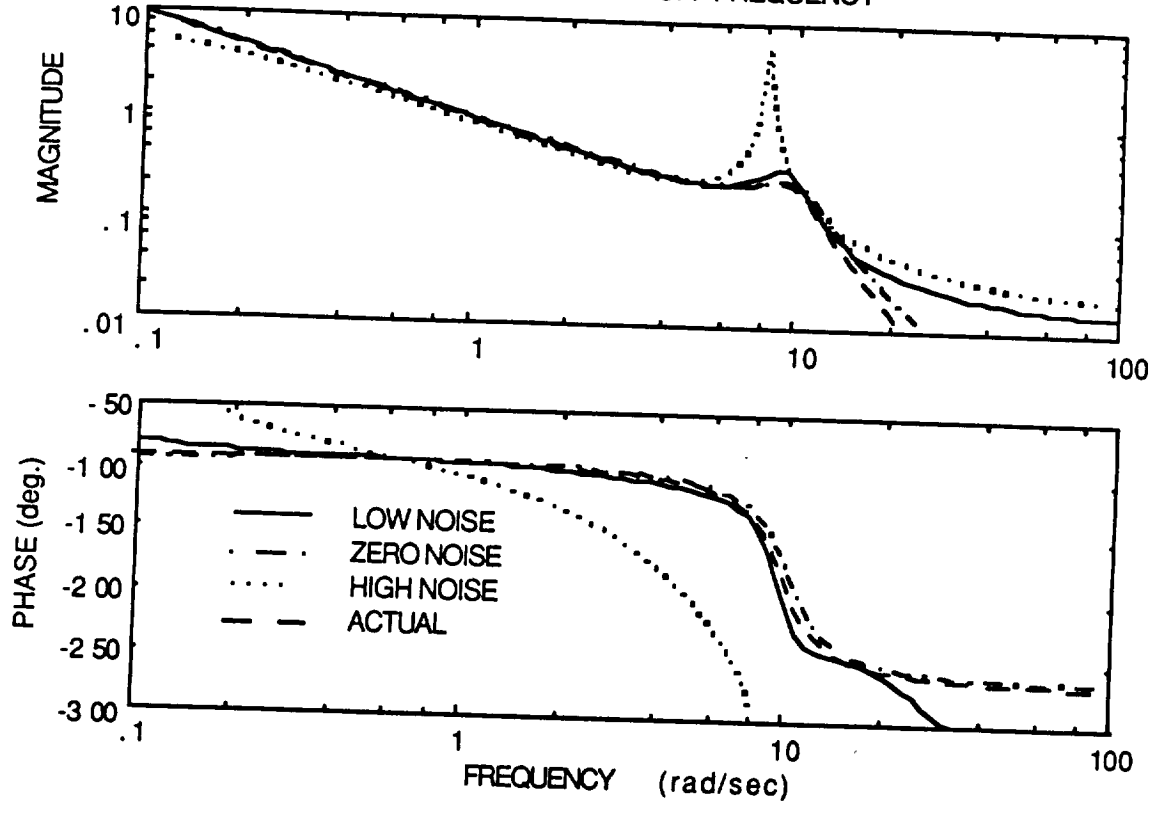


FIGURE 7 BIAS COMPARISON, MEDIUM CUTOFF FREQUENCY

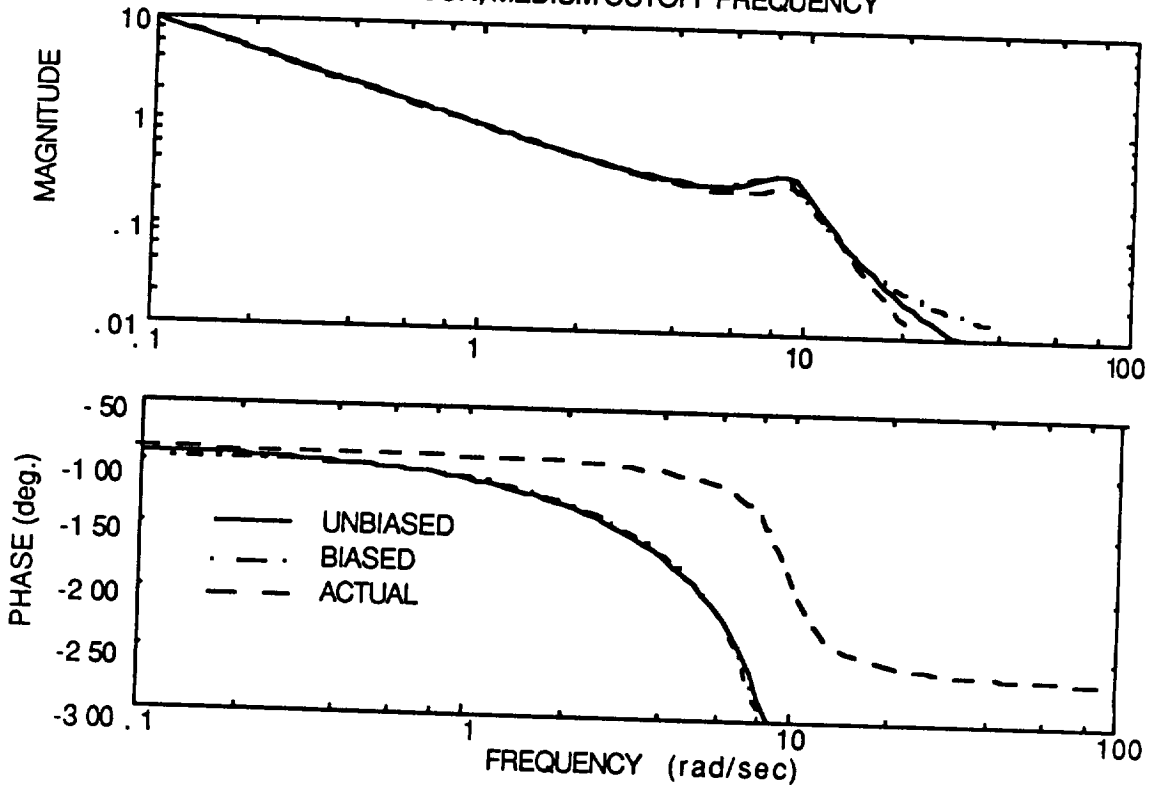


FIGURE 8 - DELAY COMPARISON, MEDIUM CUTOFF FREQUENCY.

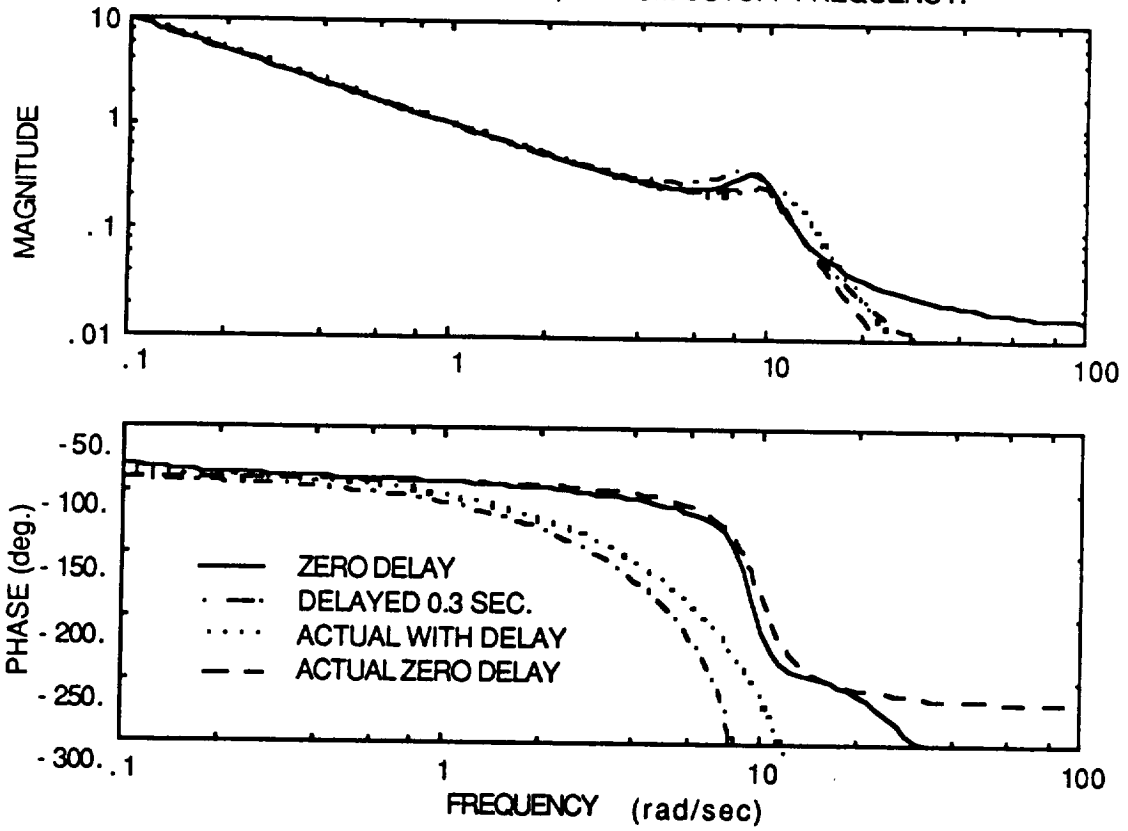


FIGURE 9 - OPEN LOOP CUTOFF COMPARISON, ZERO NOISE.

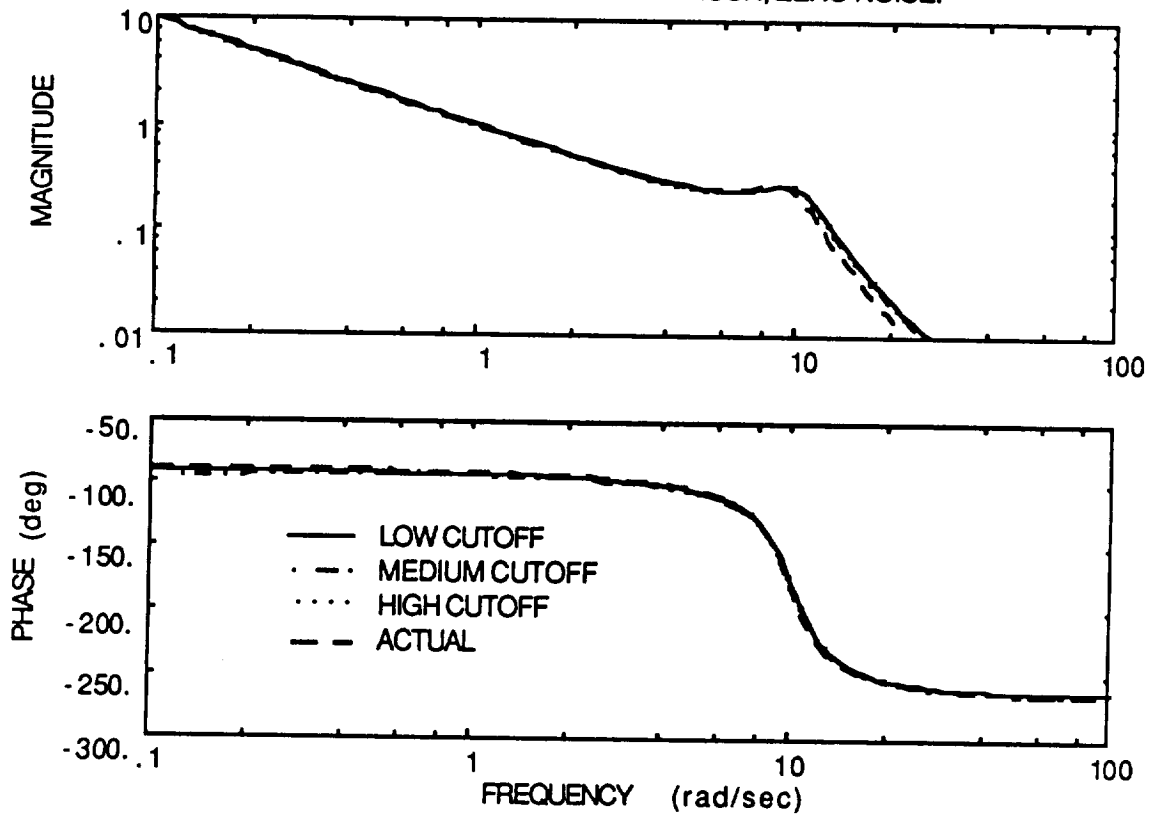


FIGURE 10 - CLOSED LOOP CUTOFF COMPARISON, ZERO NOISE

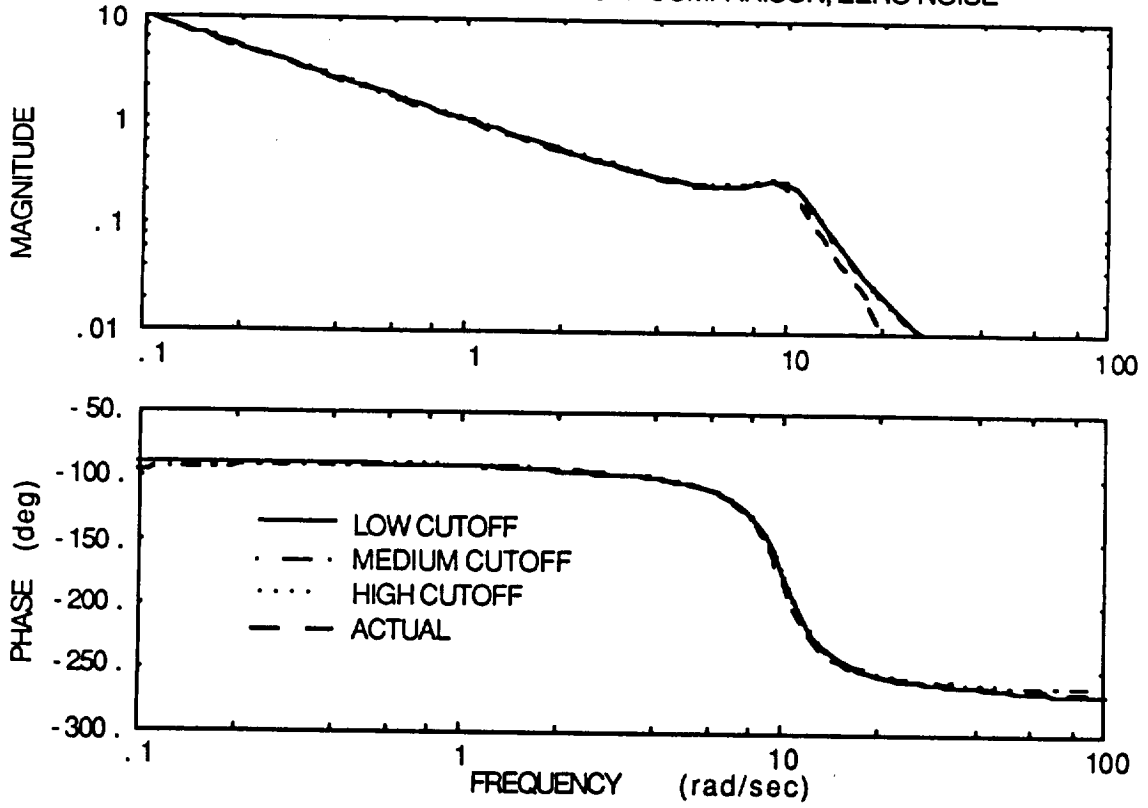


FIGURE 11 - CLOSED LOOP CUTOFF COMPARISON, WITH NOISE

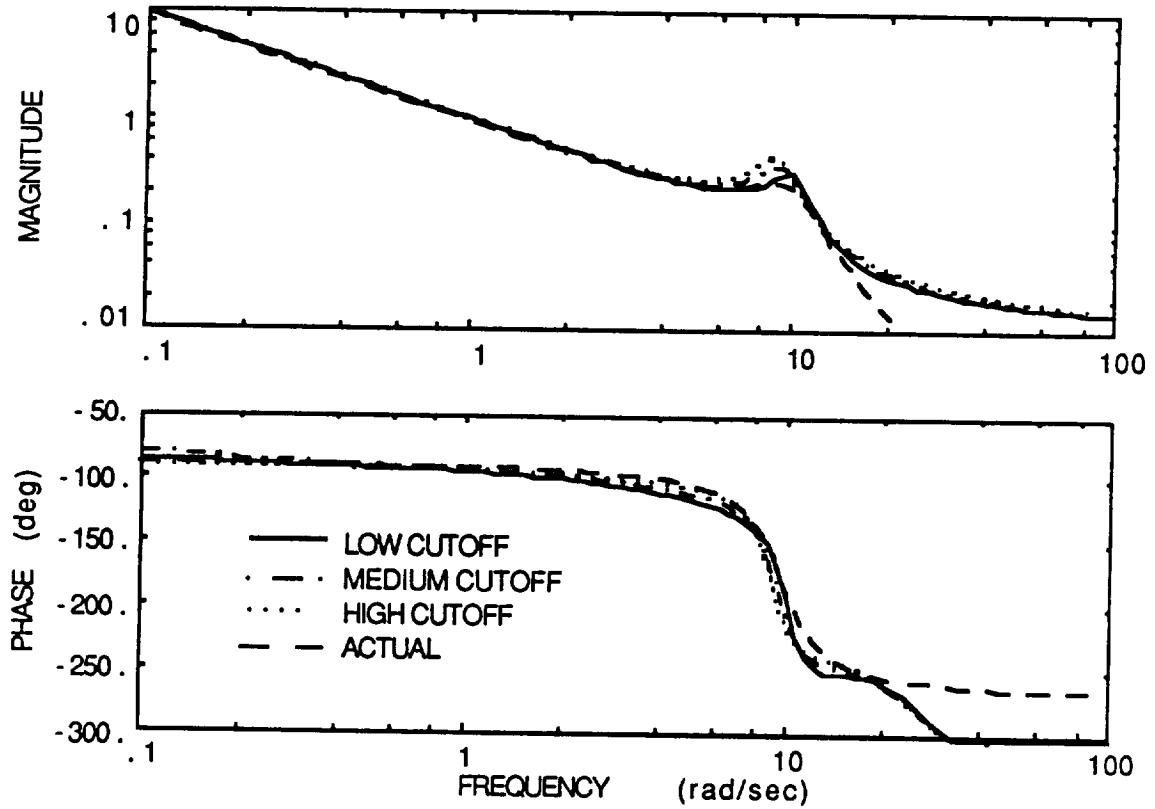


FIGURE 12 - OPEN LOOP VS. CLOSED LOOP, STEP INPUT

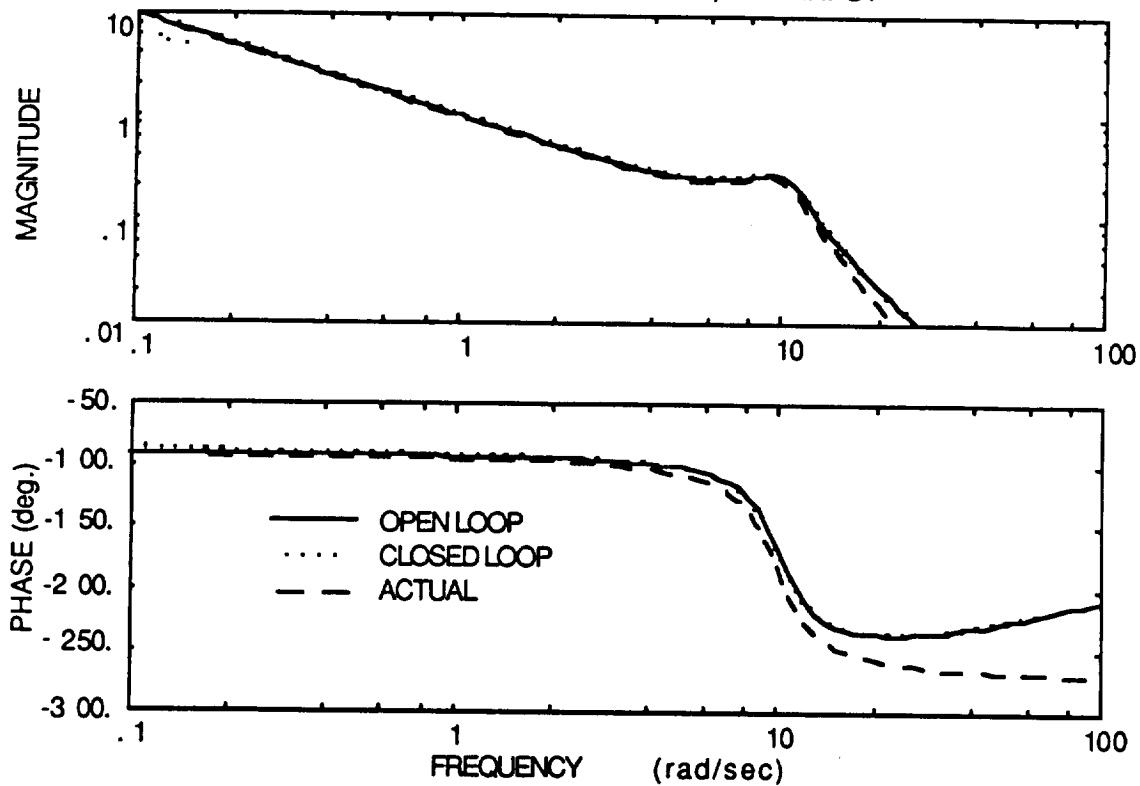


FIGURE 13 - OPEN LOOP VS. CLOSED LOOP, MEDIUM CUTOFF.

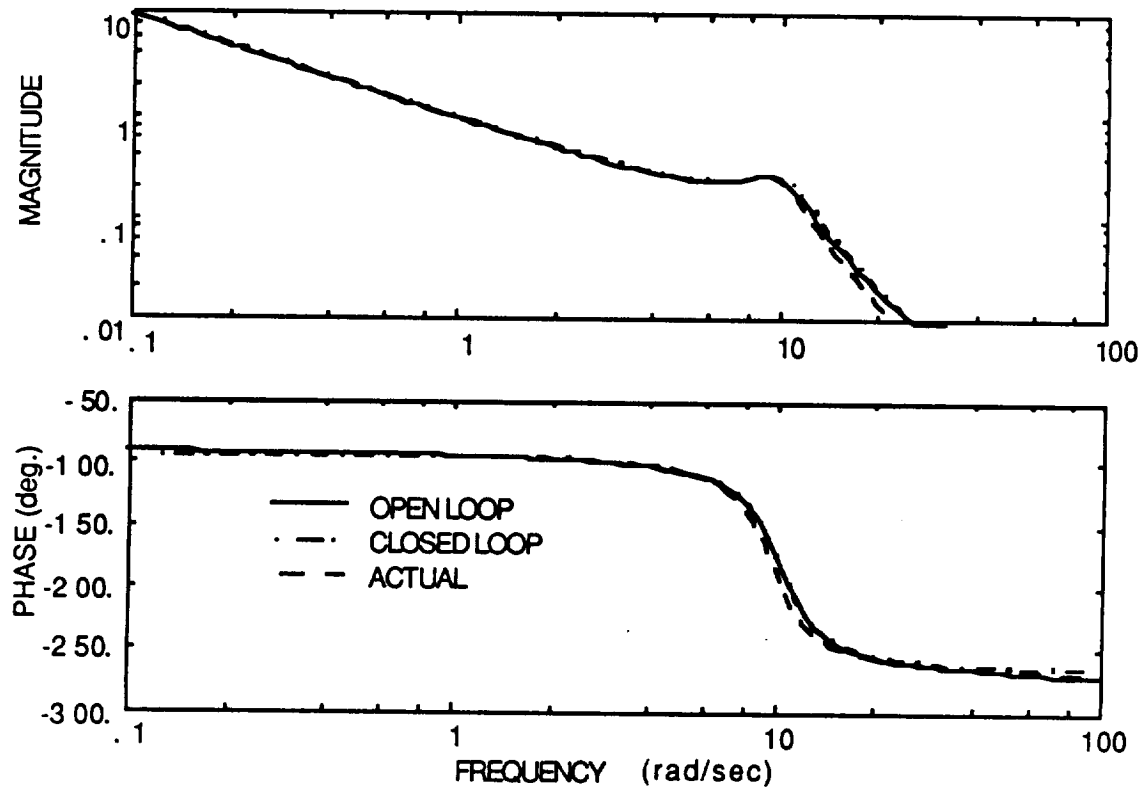


FIGURE 14 - FFT VS. LSE OPEN LOOP, MEDIUM CUTOFF. SUM OF SINES INPUT

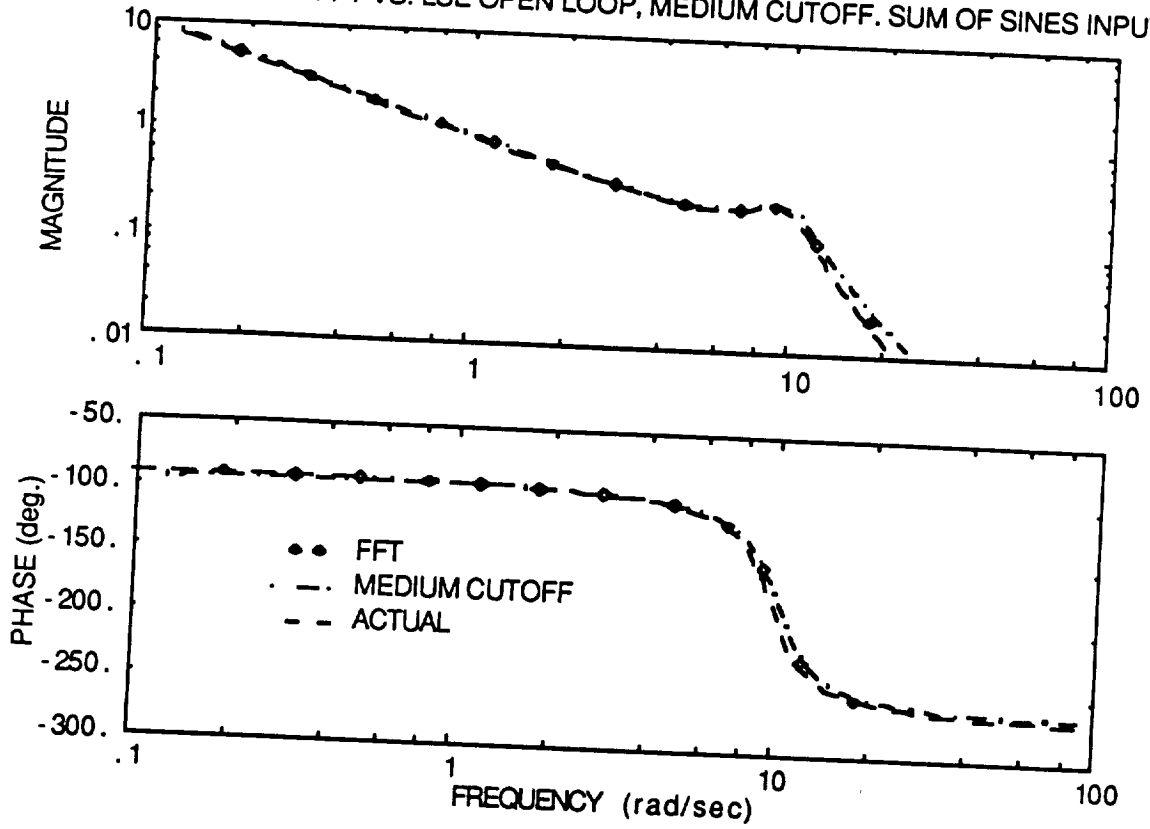


FIGURE 15 - FFT VS. LSE CLOSED LOOP, MEDIUM CUTOFF. SUM OF SINES INPUT

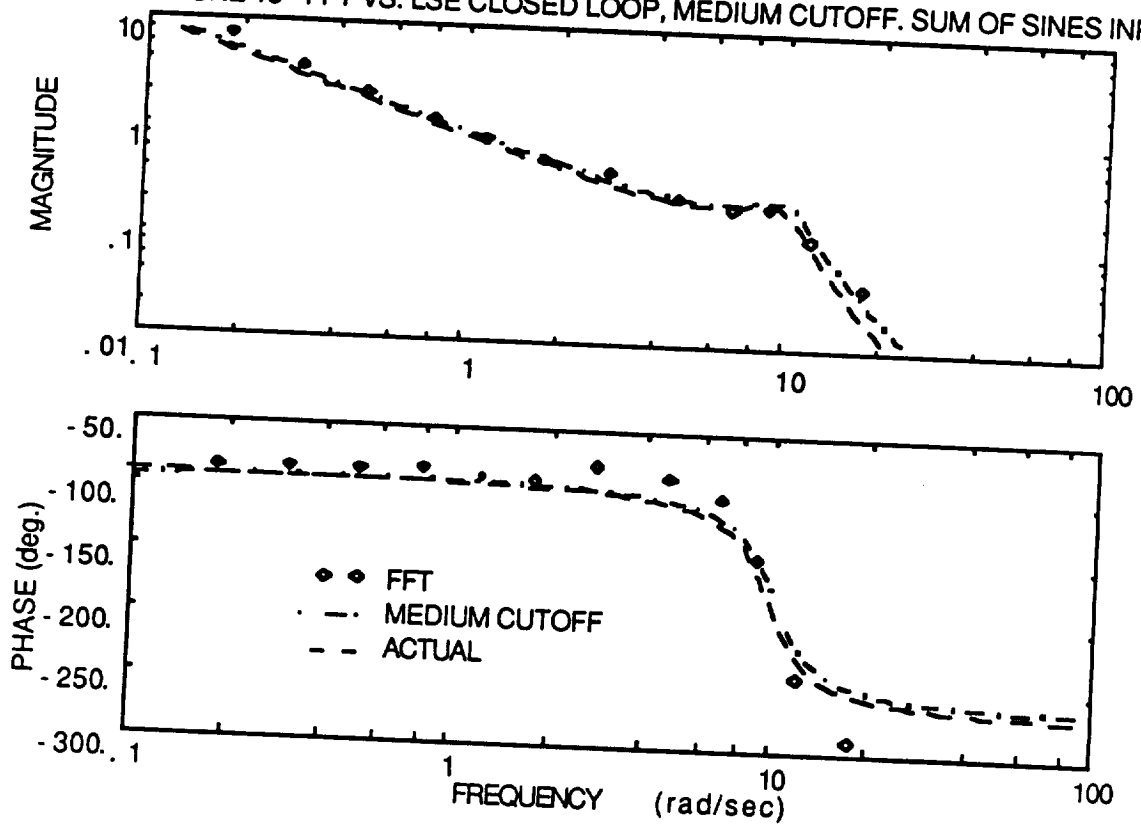


FIGURE 16 - MULTI-LOOP FFT VS. LEAST SQUARES WITH BIAS, AND ZERO NOISE

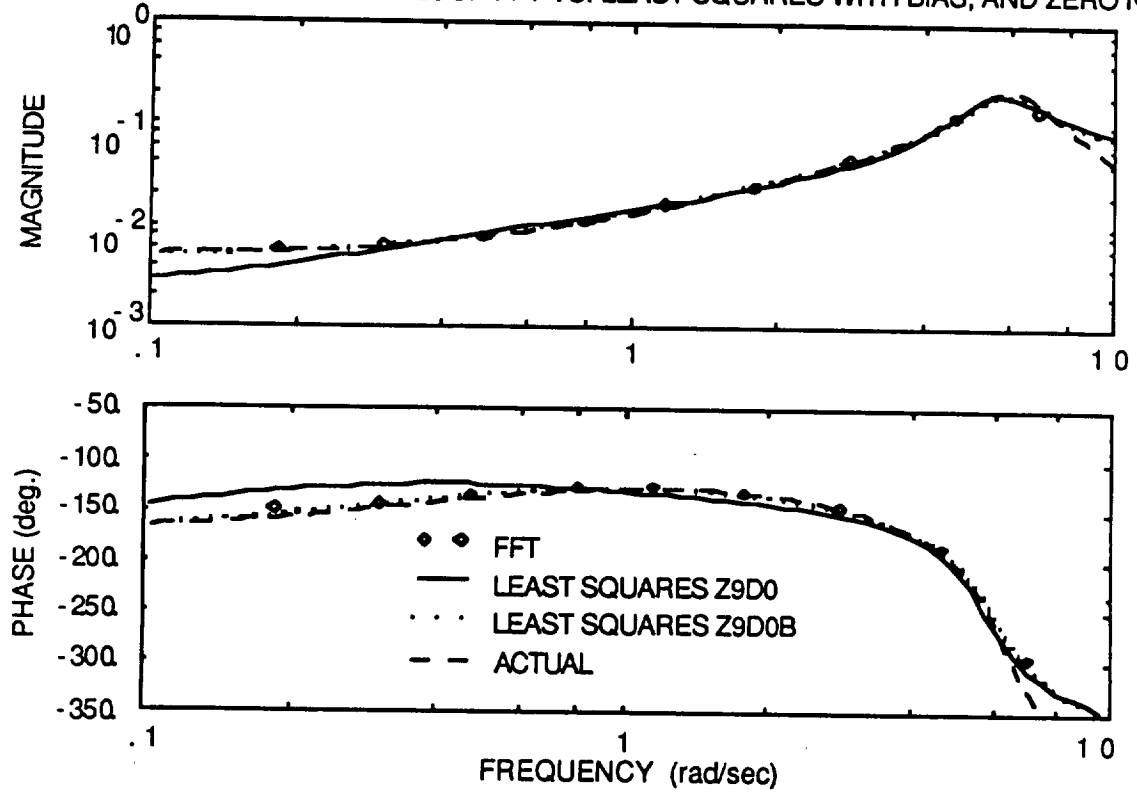
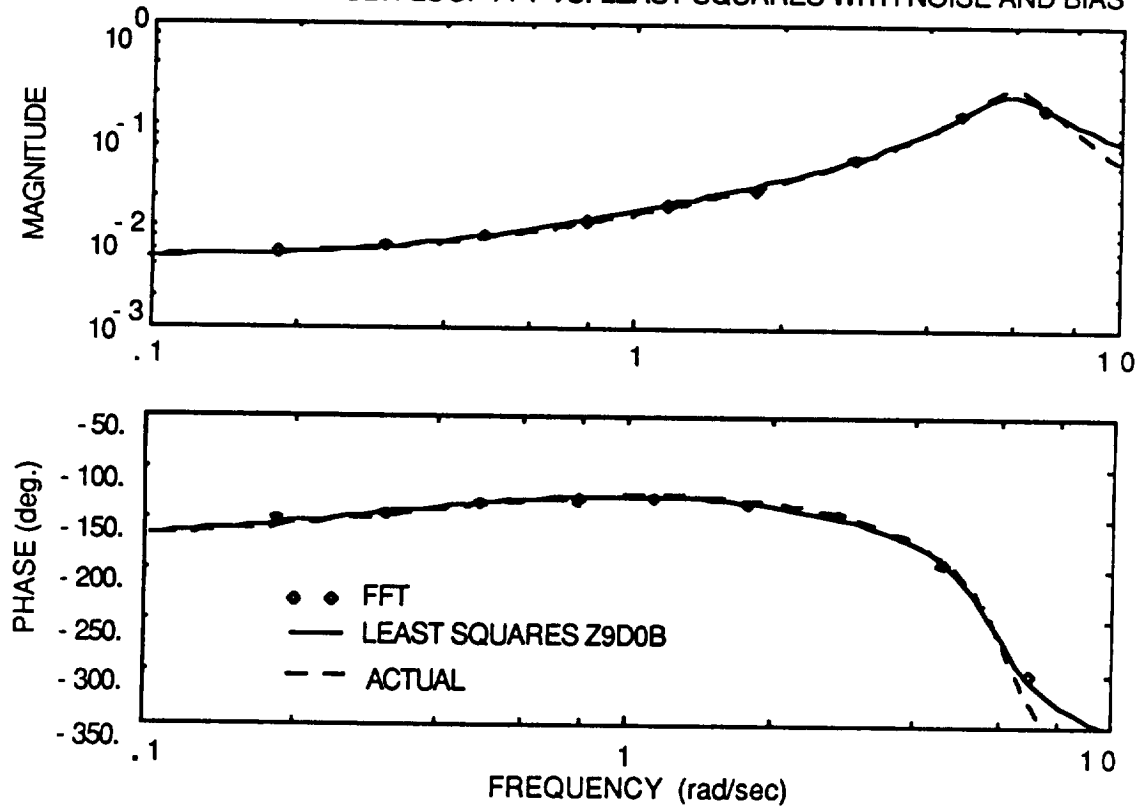


FIGURE 17 - MULTI-LOOP FFT VS. LEAST SQUARES WITH NOISE AND BIAS



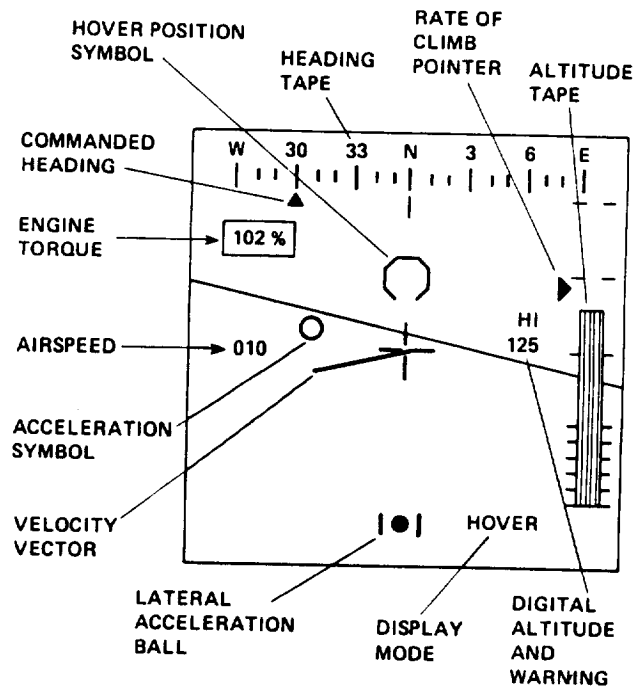


FIGURE - 18 Hover Display Symboly.

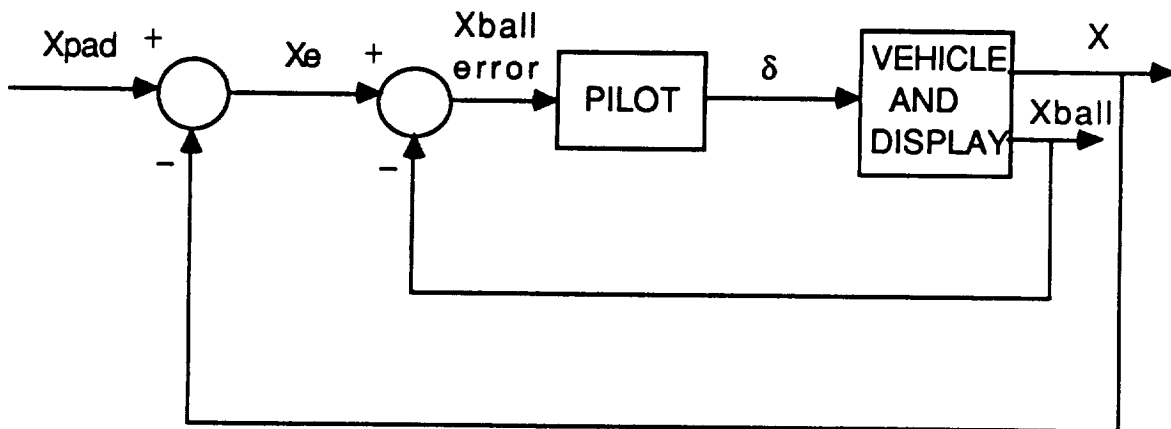
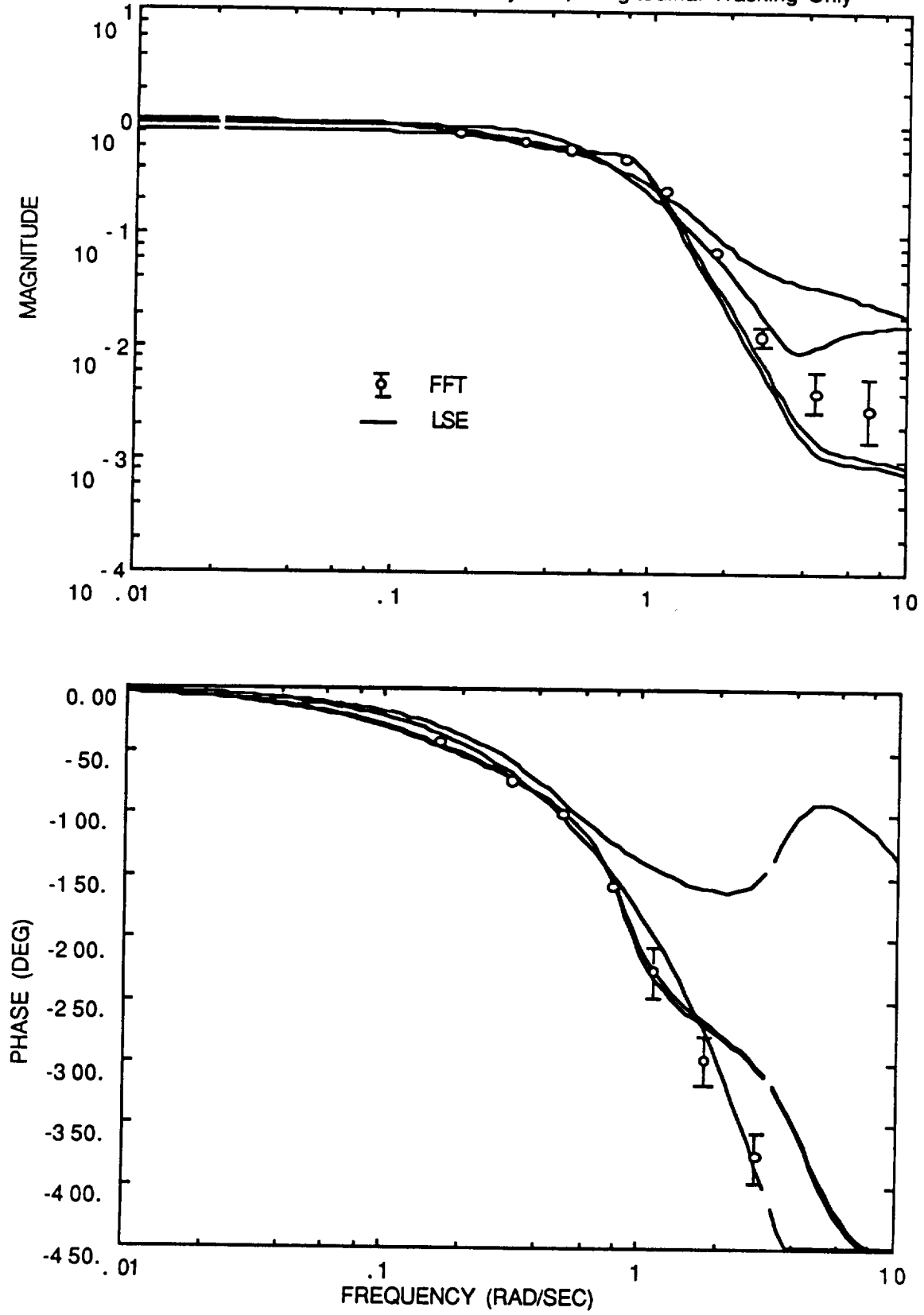


FIGURE - 19 Hypothesized pilot loop closures with acceleration ball display symboly.

FIGURE 20 - X/Xpad TF ID for Subject 1, Longitudinal Tracking Only



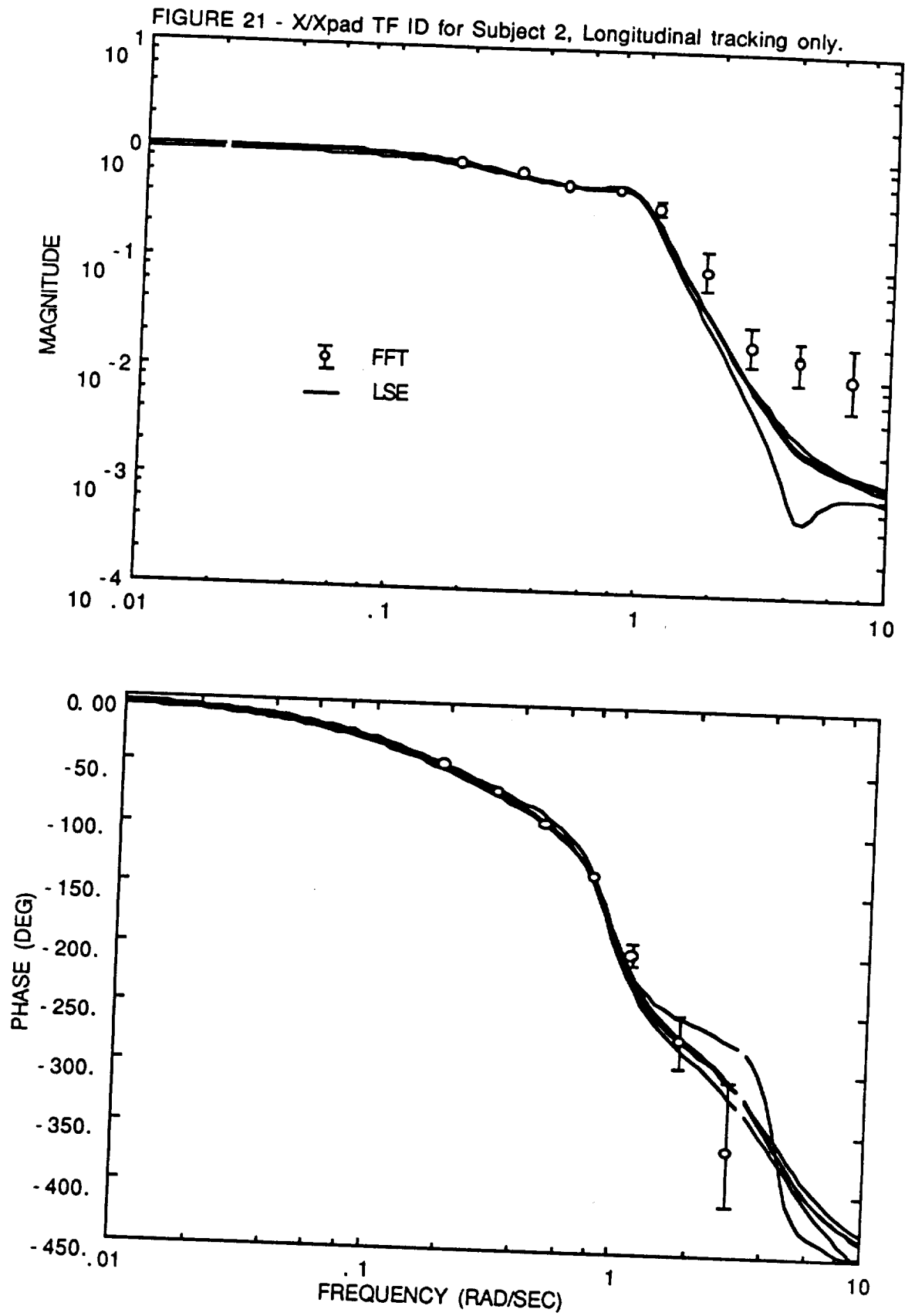


FIGURE 22 - X/Xpad TF ID for Subject 1, Lateral and longitudinal Tracking.

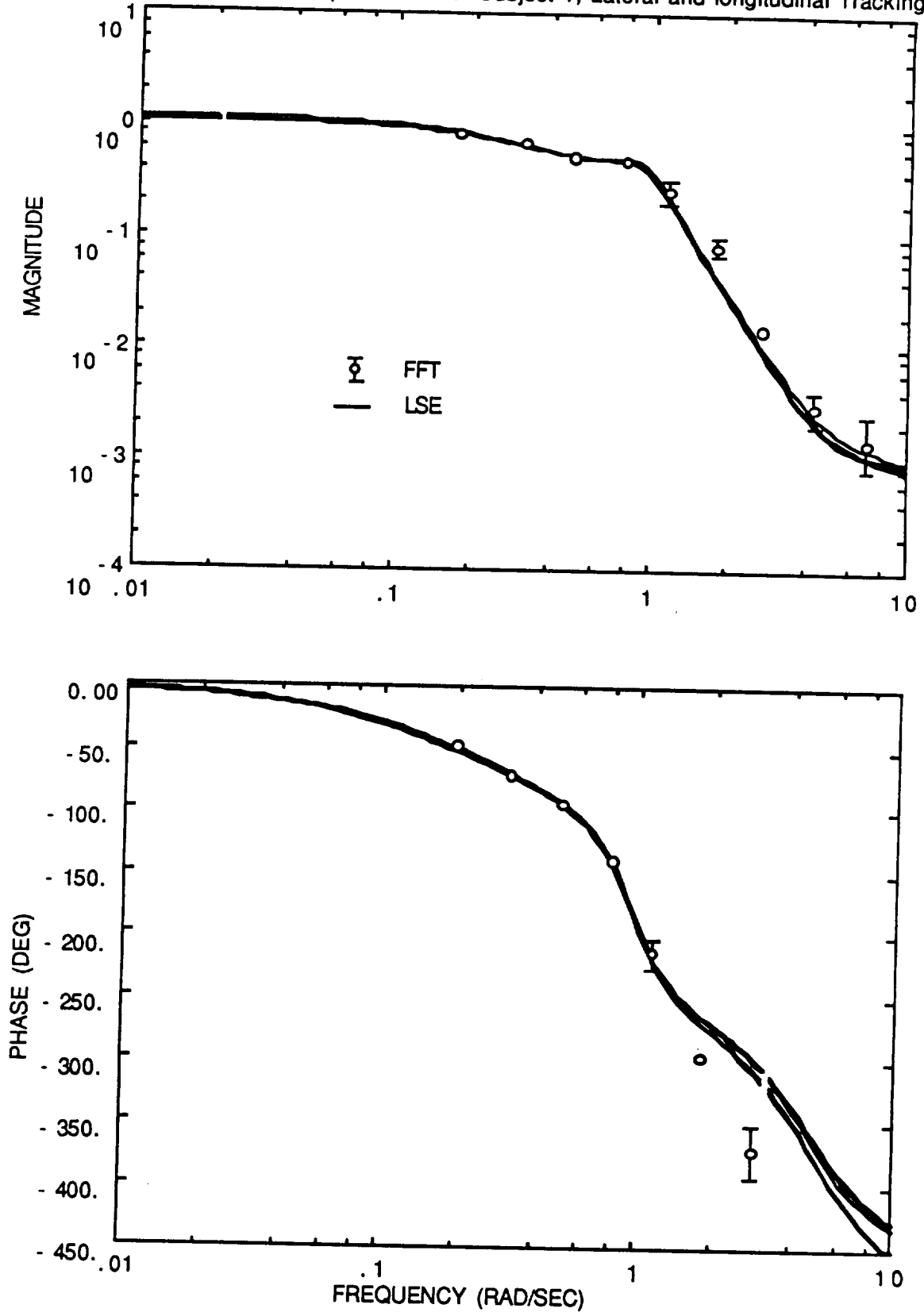


FIGURE 23 - X/Xpad TF ID for Subject 2, Lateral and longitudinal tracking.

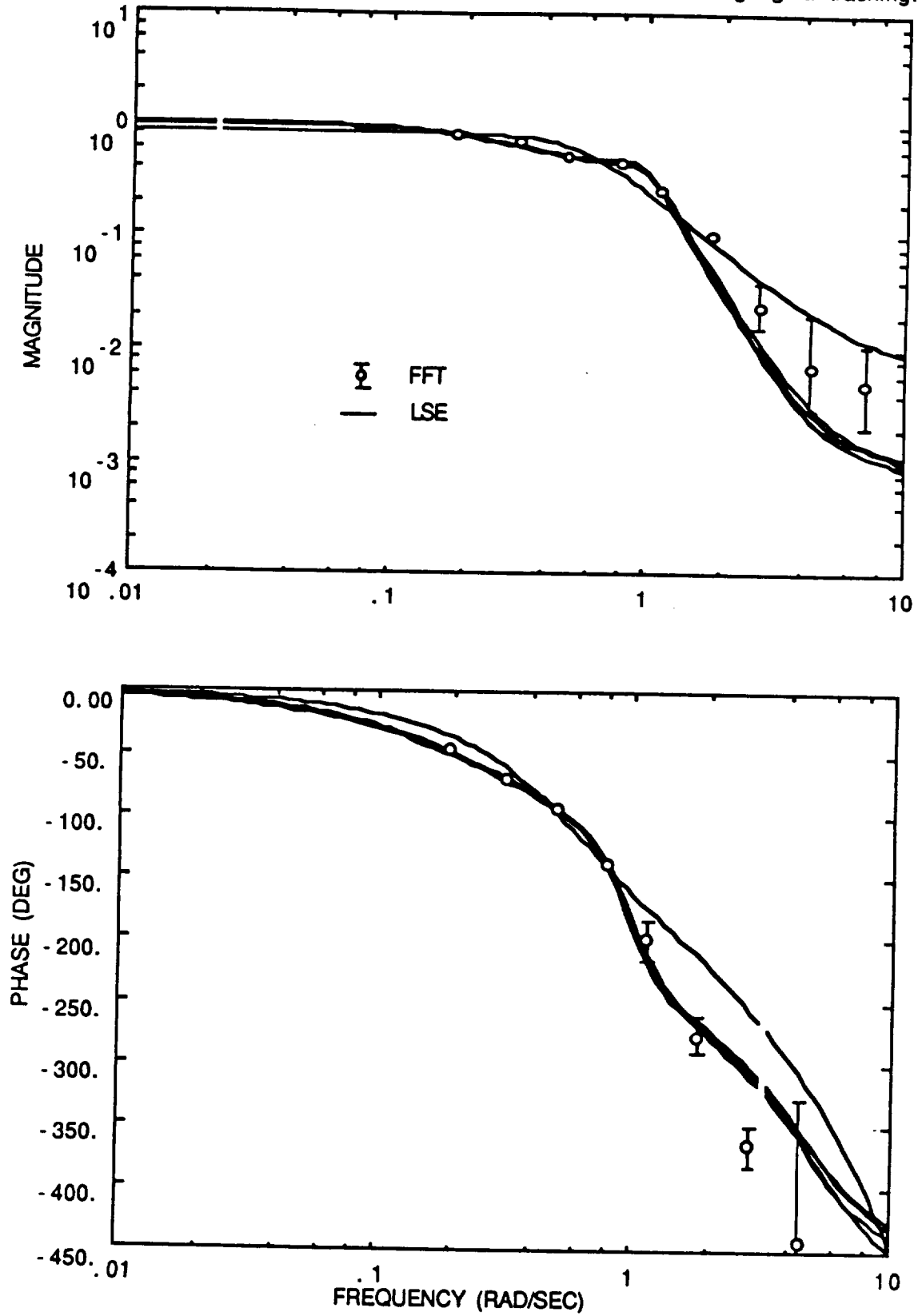


FIGURE 24 - X/Xpad TF ID for Subject 1, Lateral and longitudinal tracking without the acceleration symbol.

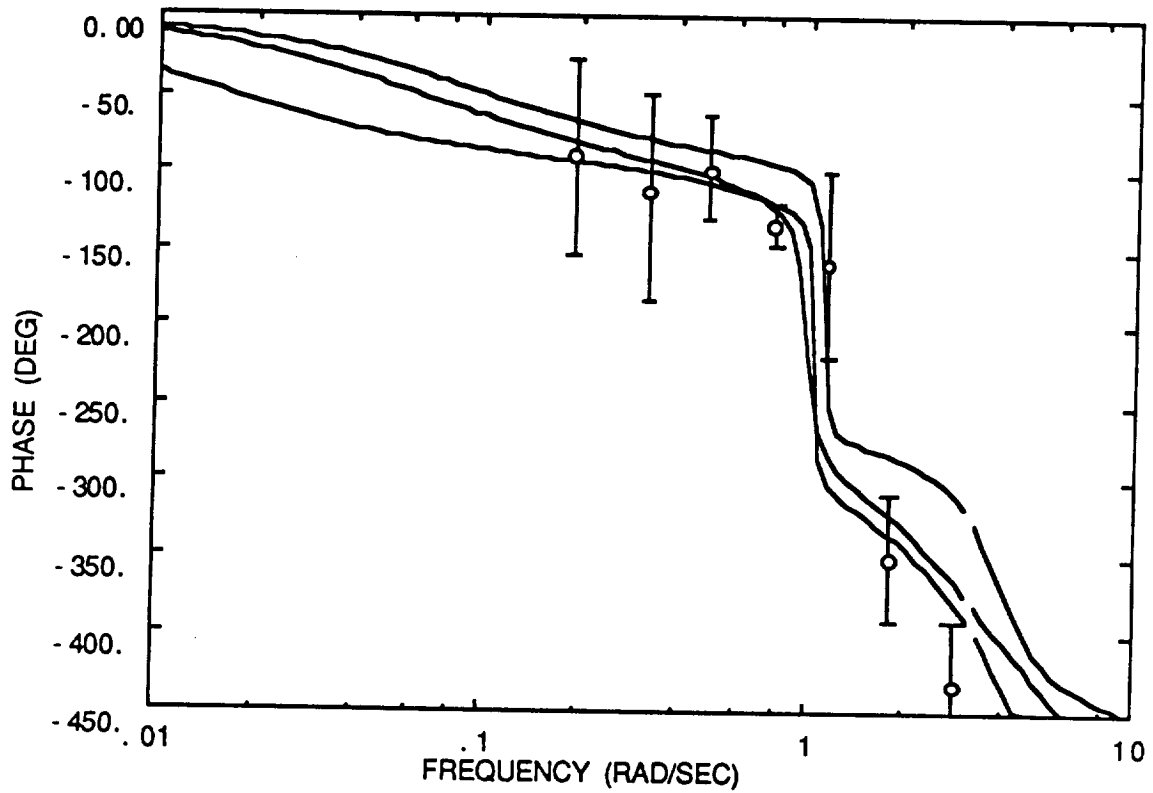
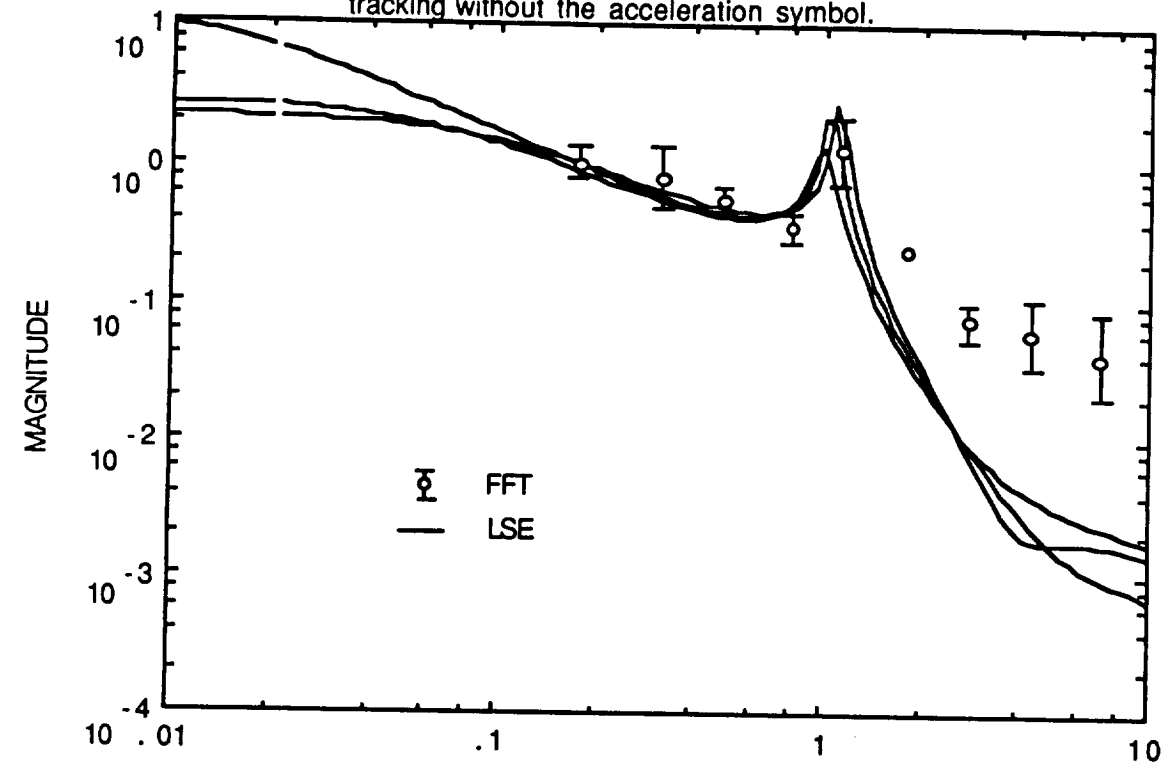


FIGURE 25 - X/Xpad TF ID for Subject 2, Lateral and longitudinal tracking without the acceleration symbol.

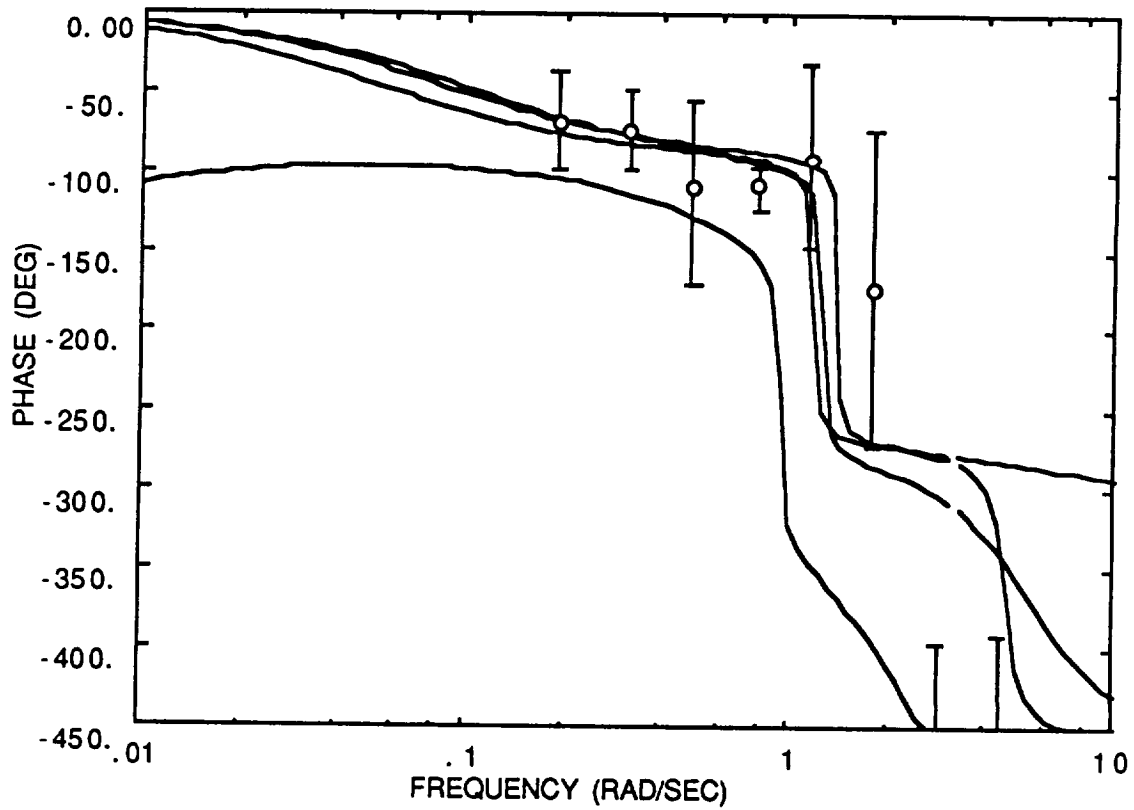
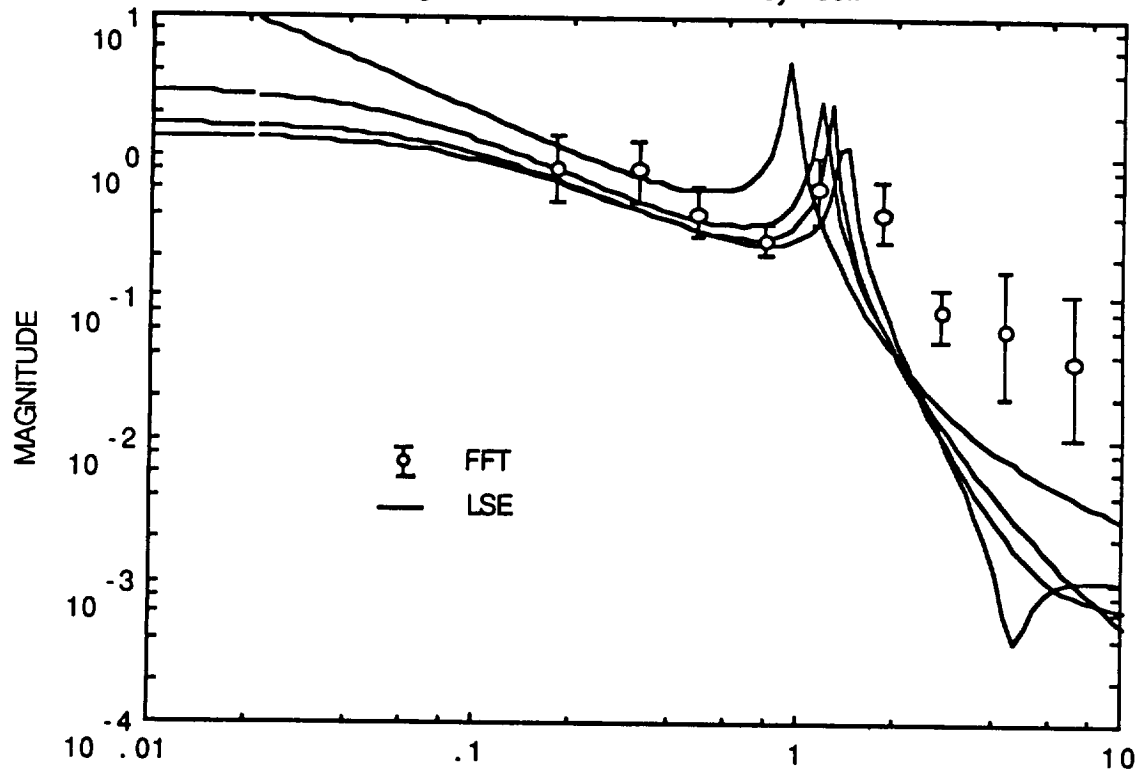


FIGURE 26 - X position vs. time plot for X/Xpad, subject 1, lateral and longitudinal tracking.

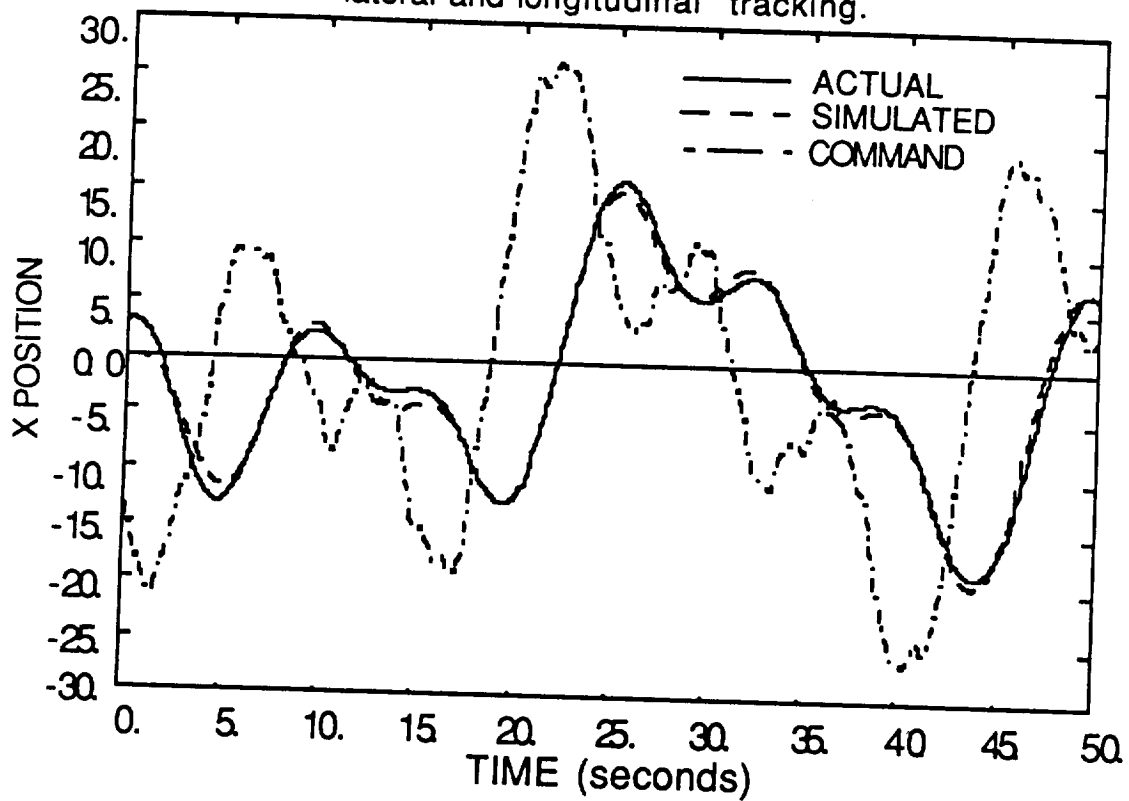


FIGURE 27 - X position vs. time plot for X/Xpad, subject 1, lateral and longitudinal tracking, no acceleration symbol.

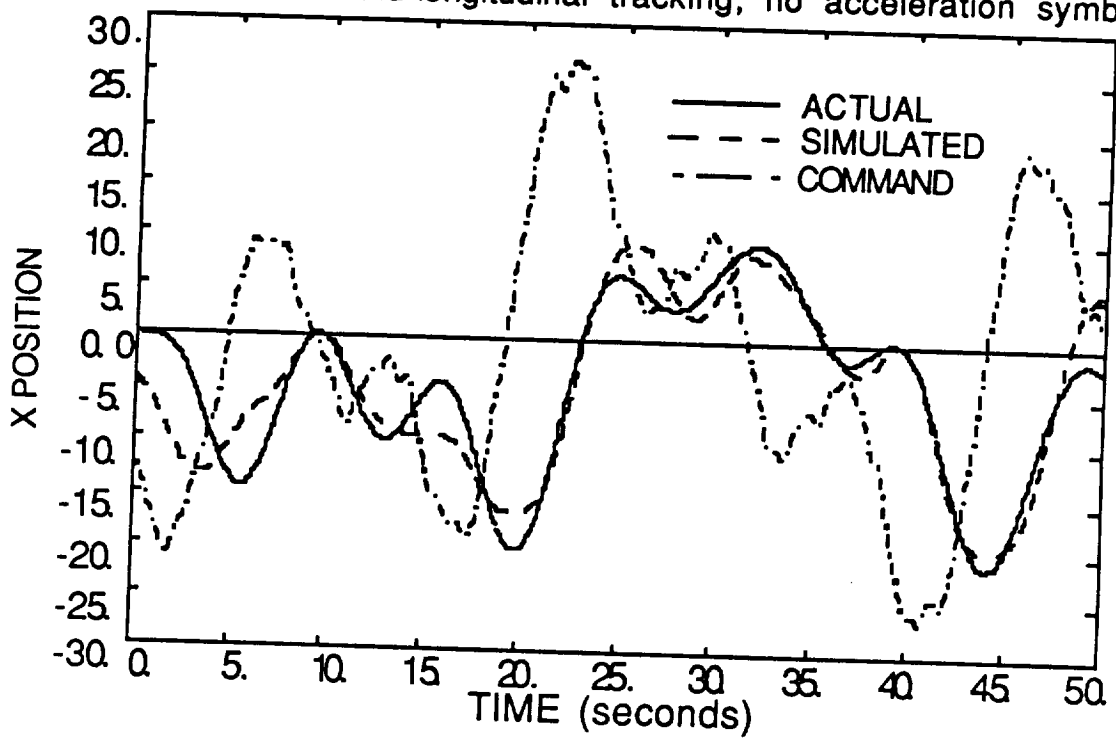


FIGURE 30 - Xball/Xball error TF ID for Subject 1, Lateral and longitudinal tracking.

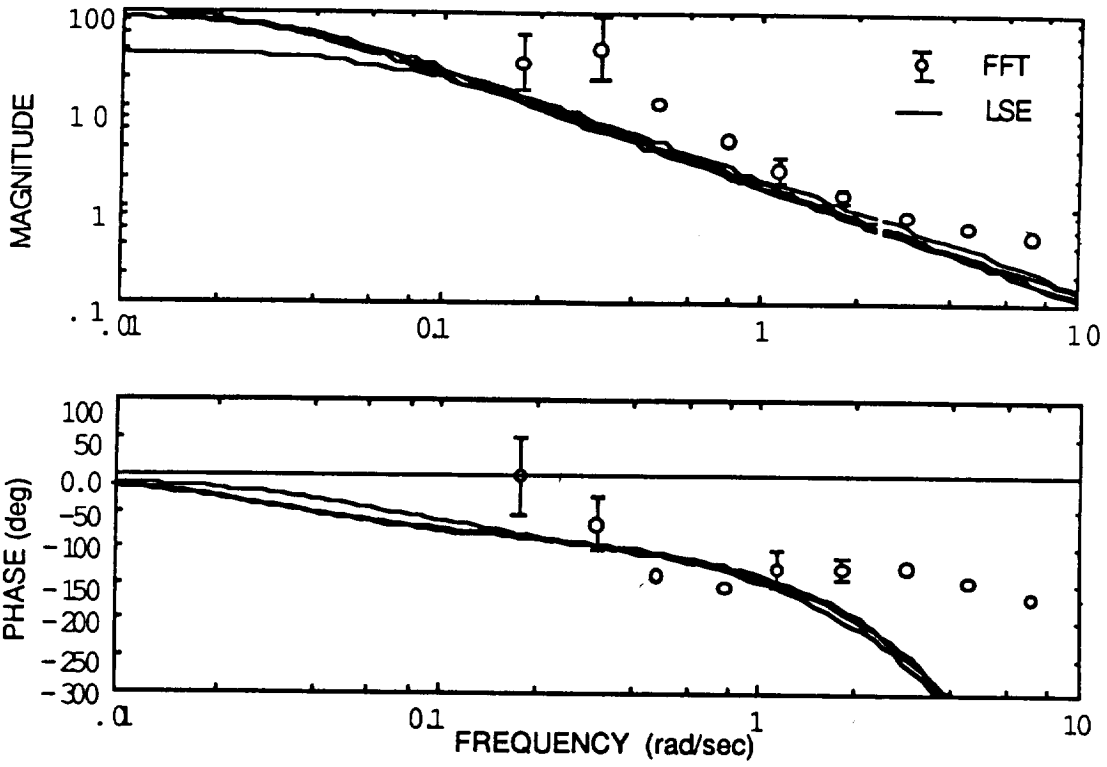
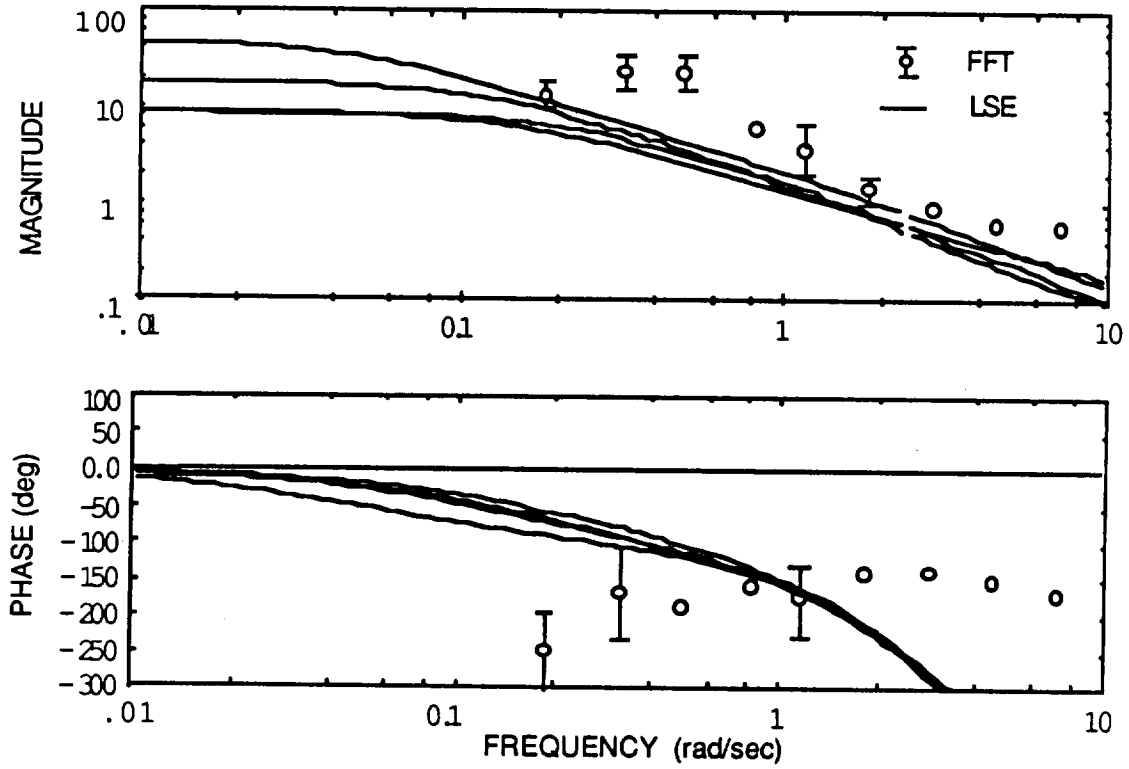


FIGURE 31 - Xball/Xball error TF ID for Subject 2, Lateral and longitudinal tracking.



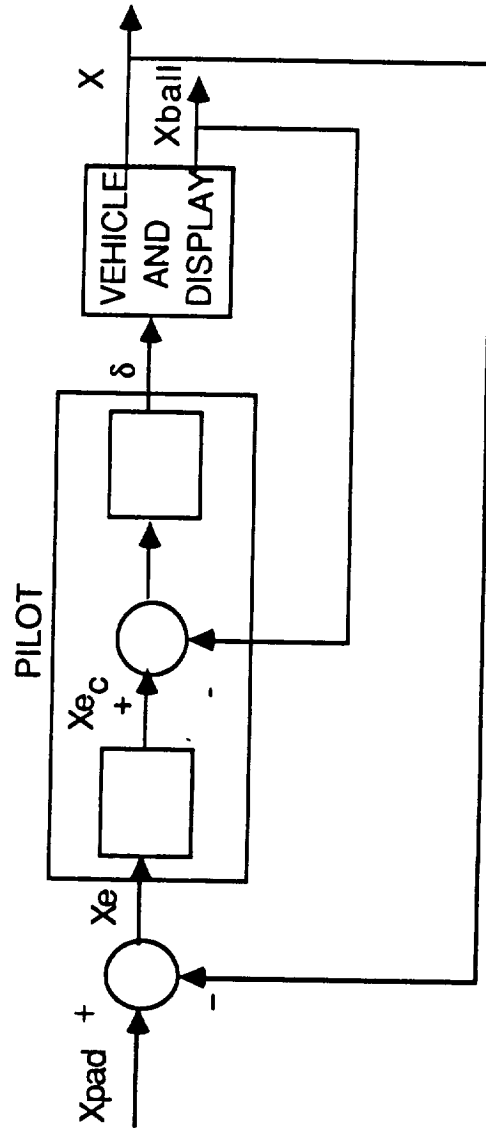


FIGURE - 32 Alternative multi-loop pilot loop closures with acceleration ball display symbology.

FIGURE 35 - Xball/Xpad TF ID for Subject 1, Lateral and longitudinal tracking.

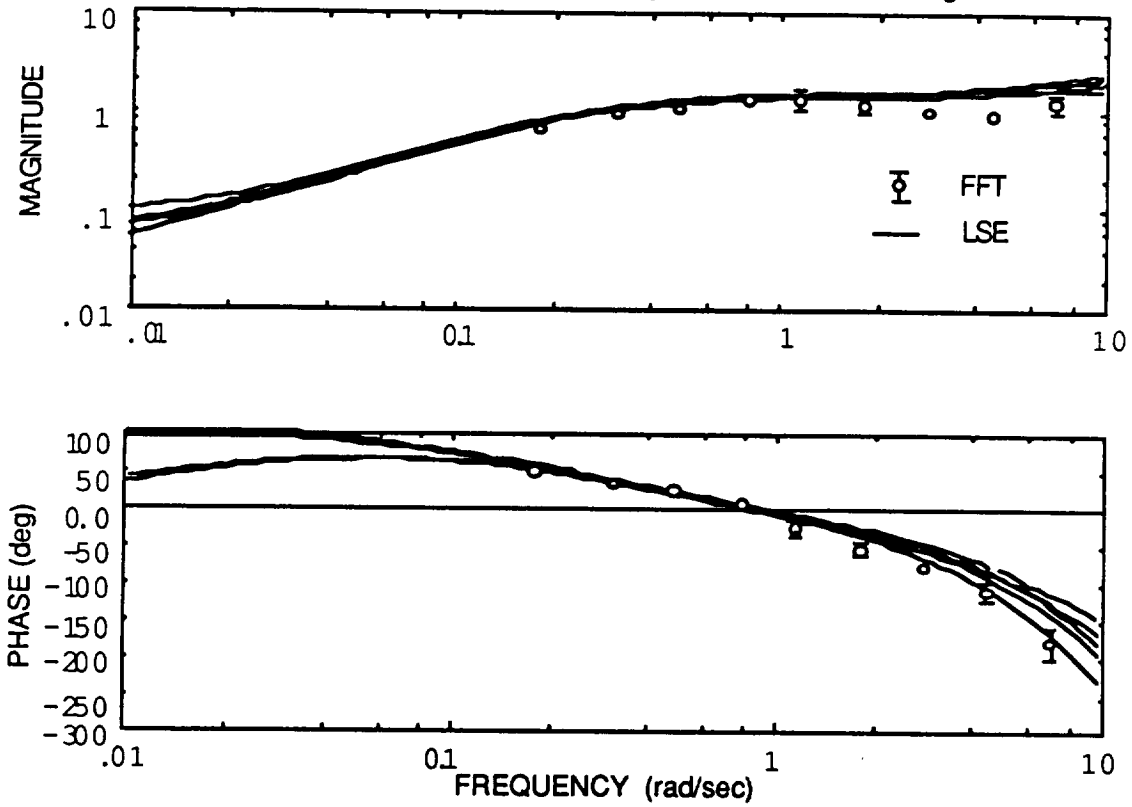
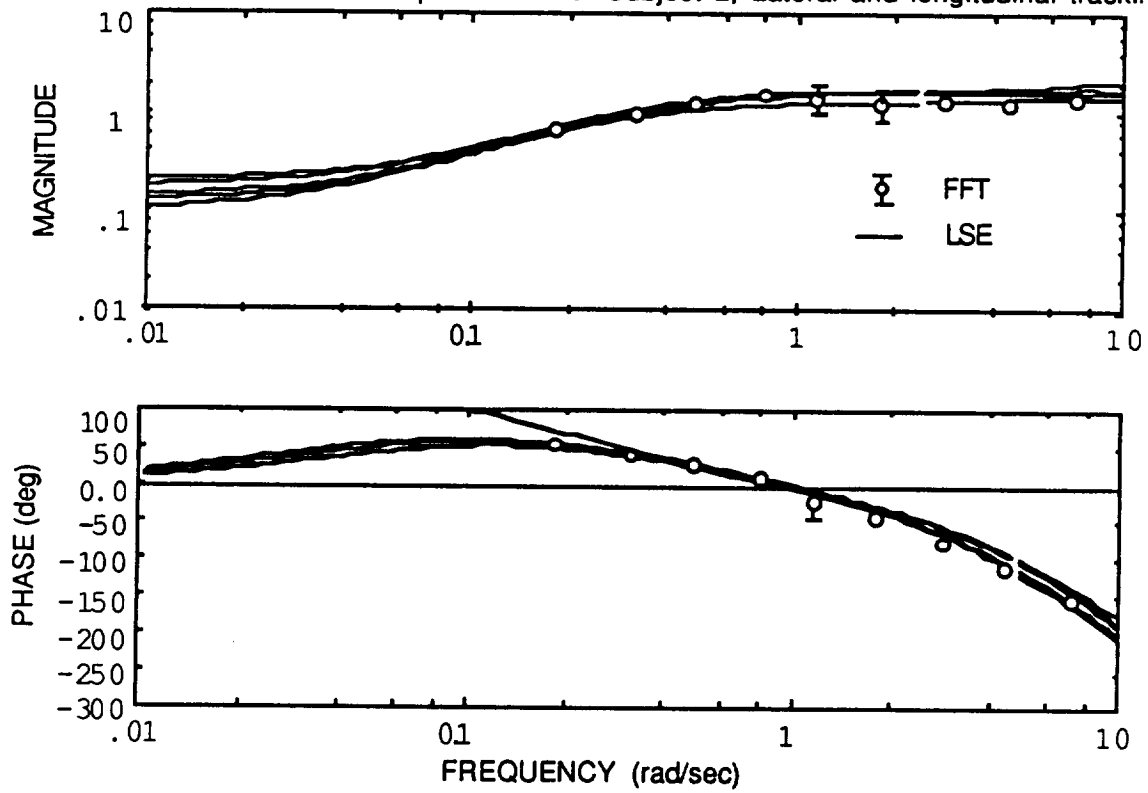
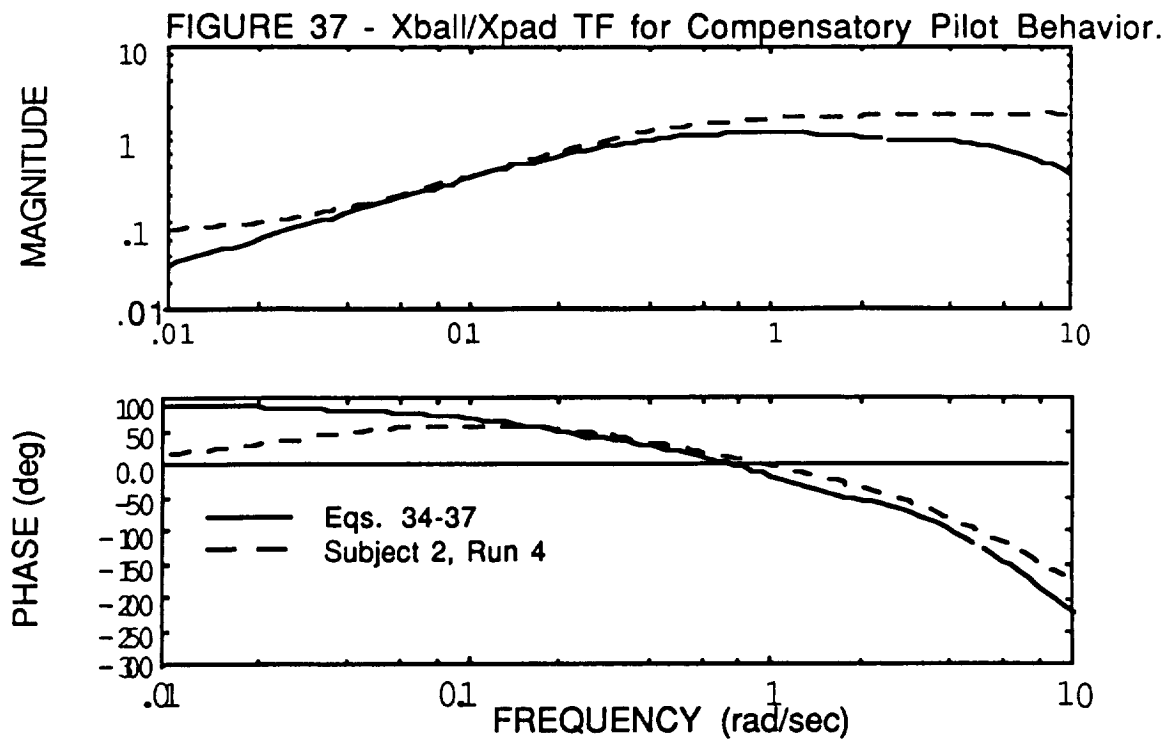


FIGURE 36 - Xball/Xpad TF ID for Subject 2, Lateral and longitudinal tracking.





8.0 Appendix III Computer Programs

**** ACSL multi-loop helicopter simulation ****

PROGRAM HELI1

**CONSTANT TFIN=110.
CONSTANT TDX=0.15
CONSTANT KEX1=1.
CONSTANT QX2=1.,14.14,100.
CONSTANT K=98.03
CONSTANT K1=1.
CONSTANT K2=10.
CONSTANT T1=2.5
CONSTANT T2=.369
CONSTANT XU=-0.05
CONSTANT G=32.2
CONSTANT MU=.0311
CONSTANT MTH=-8.
CONSTANT MDE=.585
CONSTANT MQ=-5.
CONSTANT TL=3.0
CONSTANT KY=.0071
CONSTANT ta=0.2
CONSTANT kn=1.0
CONSTANT m=0.0
CONSTANT s=0.02710
CONSTANT mn=0.00121285**

ARRAY QX2(3)

CINTERVAL CINT=0.05

**INITIAL
UNIFI(1717)
END \$ "OF INITIAL"**

**DYNAMIC
DERIVATIVE**

```

DX=TRAN(0,2,100.,QX2,U1)
UM1=(.01*T1)*LEDLAG(100.,T1,DX,0.)
"UMX1=K2*UM1"
"UMX1=(K2/T2)*LEDLAG(T2,.01,UM1,0.)"
UMX1=(K2*T2)*LEDLAG(0.,T2,UM1,0.)
U1=UCX1-UM1-UMX1
UCX1=KEX1*DELAY(X1EN,0.,TDX,300)

x1e =thc-th
X1EN=THC-TH+en+0.1
en=kn*(ou(ta,m,s)-mn)
XC=17.6*(SIN(.1841*T)+SIN(.3068*T)+SIN(.4909*T)+SIN(.7977*T)+...
    0.1*(SIN(1.166*T)+SIN(1.779*T)+SIN(2.823*T))+...
    0.05*(SIN(4.663*T)+SIN(6.934*T)))
XE=XC-X
THC=-KY*LEDLAG(TL,.01,XE,0.)
UD=XU*U-G*TH
THD=Q
QD=MU*U+MTH*TH+MQ*Q+MDE*(DX*K)
XD=U

TH=INTEG(THD,0.)
Q=INTEG(QD,0.)
U=INTEG(UD,0.)
X=INTEG(XD,0.)

TP=1./TFIN
VX1E=TP*INTEG(X1E**2.,0.)
VTHC=TP*INTEG(THC**2.,0.)
VXC=TP*INTEG(XC**2.,0.)
VX=TP*INTEG(X**2.,0.)
VDX=TP*INTEG(DX**2.,0.)
nbar=tp*integ(en,0.)
END $ "OF DERIVATIVE"

TERMT(T .GE. TFIN)

END $ "OF DYNAMIC"
END $ "OF PROGRAM"

```

** ACSL closed-loop simulation, sum of sines input with noise, **
 ** delay , and bias. **

```

program ndbsin
array d(4)
constant d=1.,4.,100.,0., ta=0.2, kn=1.0, mn=0.00236539, m=0., s=0.03215
constant w1=0.1841, w2=0.3068, w3=0.4909, w4=0.7977, w5=1.166
constant w6=1.779, w7=2.823, w8=4.663, w9=6.933, w10=8.958
constant w11=12.088, w12=17.978, td=0.3
tfin=102.4
cinterval cint=0.05
INITIAL
UNIFI(3333)
END $"OF INITIAL"
dynamic
derivative
ed=delay(e1+n,0.,td,300)
c=tran(0,3,100.,d,ed)
e1=r-c+1.
e=e1-1.
n=kn*(ou(ta,m,s)-mn)
r=(sin(w1*t)+sin(w2*t)+sin(w3*t)+0.1*(sin(w4*t)+sin(w5*t)+...
sin(w6*t)+sin(w7*t)+sin(w8*t)+sin(w9*t)+sin(w10*t)+...
sin(w11*t)+sin(w12*t)))/1.546
tf=1./tfin
nbar=tf*integ(n,0.)
end $ "of derivative"
end $ "of dynamic"
termt(t.ge.tfin)
end $ "of program"

```

```

** ACSL closed-loop simulation, sum of sines input with noise, **
**                               and delay .                               **

```

```

program ndsin
array d(4)
constant d=1.,4.,100.,0., ta=0.2, kn=1.0, mn=0.00303933, m=0.0, s=0.04131
constant w1=0.1841, w2=0.3068, w3=0.4909, w4=0.7977, w5=1.166
constant w6=1.779, w7=2.823, w8=4.663, w9=6.933, w10=8.958
constant w11=12.088, w12=17.978, td=0.3
tfin=102.4
cinterval cint=0.05
INITIAL
UNIFI(3333)
END $"OF INITIAL"
dynamic
derivative
ed=delay(e+n,0.,td,300)
c=tran(0,3,100.,d,ed)
e=r-c
n=kn*(ou(ta,m,s)-mn)
r=(sin(w1*t)+sin(w2*t)+sin(w3*t)+sin(w4*t)+sin(w5*t)+...
sin(w6*t)+0.1*(sin(w7*t)+sin(w8*t)+sin(w9*t)+sin(w10*t)+...
sin(w11*t)+sin(w12*t)))/3.03
tf=1./tfin
nbar=tf*integ(n,0.)
end $ "of derivative"
end $ "of dynamic"
termt(t.ge.tfin)
end $ "of program"

```

```

** ACSL closed-loop simulation, sum of sines input with noise. **

program nsin
array d(4)
constant d=1.,4.,100.,0., ta=0.1, kn=1.0, mn=0.05276090, m=0., s=1.0
constant w1=0.1841, w2=0.3068, w3=0.4909, w4=0.7977, w5=1.166
constant w6=1.779, w7=2.823, w8=4.663, w9=6.933, w10=8.958
constant w11=12.088, w12=17.978
tfin=102.4
cinterval cint=0.05
INITIAL
UNIFI(3333)
END $"OF INITIAL"
dynamic
derivative
c=tran(0,3,100.,d,e+n)
e=r-c
n=kn*(ou(ta,m,s)-mn)
r=(sin(w1*t)+sin(w2*t)+sin(w3*t)+sin(w4*t)+sin(w5*t)+...
sin(w6*t)+0.1*(sin(w7*t)+sin(w8*t)+sin(w9*t)+sin(w10*t)+...
sin(w11*t)+sin(w12*t)))/3.03
tf=1./tfin
nbar=tf*integ(n,0.)
end $ "of derivative"
end $ "of dynamic"
termt(t.ge.tfin)
end $ "of program"

```

** ACSL closed-loop simulation with sum of sines input. **

```

program sin
array d(4)
constant d=1.,4.,100.,0.
CONSTANT w1=0.1841, w2=0.3068, w3= 0.4909, w4=0.7977, w5=1.166
constant w6=1.779, w7=2.823, w8=4.663, w9=6.933
CONSTANT W10=8.958, W11=12.088, W12=17.978
tfin=102.4
cinterval cint=0.05
dynamic
derivative
c=tran(0,3,100.,d,e)
e=r-c
r=(sin(w1*t)+sin(w2*t)+sin(w3*t)+sin(w4*t)+sin(w5*t)+...
sin(w6*t)+sin(w7*t)+sin(w8*t)+0.1*(sin(w9*t)+sin(w10*t)+...
sin(w11*t)+sin(w12*t)))/4.02
end $ "of derivative"
end $ "of dynamic"
termt(t.ge.tfin)

end $ "of program"

```

```

// *** z-domain to w'-domain transformation subroutine ***
T=0.05;
ZZ=SIZE(NU);
N=ZZ(1,2)-1;
X = [T/2 1];
Y = [-T/2 1];
K=N+1;
A=0*ONES(N,K);
B=0*ONES(N,K);
C=0;D=0;DD=0;CC=0;NUM=0;DEN=0;
YY=1;M=1;XX=1;
  FOR I=1:K;...
    FOR J=1:M;...
      L=J+K-I;...
      A(I,L)=XX(1,J);...
      B(I,L)=YY(1,J);...
    END;...
    XX=CONV(XX,X);...
    YY=CONV(YY,Y);...
    M=M+1;...
  END;
Q=K;
  FOR P=1:K;...
    C(P,:)=NU(1,P)*CONV(A(Q,:),B(P,:));...
    D(P,:)=DE(1,P)*CONV(A(Q,:),B(P,:));...
    Q=K-P;...
  END;
CC=C';DD=D';S=2*N+1;Q2=K;
  FOR R=1:K;...
    NUM(1,Q2)=SUM(CC(S,:));...
    DEN(1,Q2)=SUM(DD(S,:));...
    Q2=K-R;...
    S=S-1;...
  END;
NUM,DEN
n=NUM;
q=DEN;
PAGE

```

```
[a,b,c,d]=tf2ss(n,q);  
v=logspace(-1,2);  
[mag,pha]=bode(a,b,c,d,1,v);  
WINDOW('211')  
a=[0.1,0.01;100,10;33.3,3.33];  
plot(a,'scale')  
plot(v,mag,'loglog','dotted')  
title('magnitude','  ')  
WINDOW('212')  
aa=[0.1,-300;100,-50;33.3,50];  
plot(aa,'scale')  
plot(v,pha,'logx','dotted')  
title('phase','  ')
```

```

// *** PROGRAM FAST FOURIER TRANSFORM subroutine ***
LOAD H <RRR -A;
T=H(153:2200,1);
E=H(153:2200,2);
C=H(153:2200,3);
R=H(153:2200,4);
FFTC=FFT(C);
FFTE=FFT(E);
FFTR=FFT(R);
W=[.1841;.3068;.4909;.7977;1.166;1.779;
2.823;4.663;6.934];
FOR F=1:9;...
  N=ROUND(W(F)*2048/(20*2*PI)+1);...
  MAGC(F)=SQRT((REAL(FFTC(N)))**2+(IMAG(FFTC(N)))**2);...
  MAGE(F)=SQRT((REAL(FFTE(N)))**2+(IMAG(FFTE(N)))**2);...
  PHAC(F)=180*ATAN(IMAG(FFTC(N))/REAL(FFTC(N)))/PI;...
  PHAE(F)=180*ATAN(IMAG(FFTE(N))/REAL(FFTE(N)))/PI;...
  MDB(F)=(MAGC(F)/MAGE(F));...
END;
FOR E=1:9;...
  N=ROUND(W(E)*2048/(20*2*PI)+1);...
  IF REAL(FFTC(N)) < 0. ,PHAC(E)=PHAC(E)+180.;...
END;
FOR H=1:9;...
  N=ROUND(W(H)*2048/(20*2*PI)+1);...
  IF REAL(FFTE(N)) < 0. ,PHAE(H)=PHAE(H)+180.;...
END;
FOR G=1:9;...
  IF PHAC(G) < 0. , PHAC(G)=PHAC(G)+360.;...
END;
FOR K=1:9;...
  IF PHAE(K) < 0. , PHAE(K)=PHAE(K)+360.;...
END;
PHAS = PHAC-PHAE;
A=[.1 .0001;10 1;4.95 .250];
PAGE

```

```
WINDOW('211')  
//PLOT(A,'SCALE')  
PLOT(W,MDB,'POINT=2','LOGLOG')  
YLABEL('MAGNITUDE')  
TITLE('FFT')  
WINDOW('212')  
PLOT('SCALE')  
PLOT(W,PHAS,'POINT=2','LOGX')  
YLABEL('PHASE')  
XLABEL('FREQUENCY RAD/SEC')
```

```
// ** z8d0b; LSE identification using model 8, zero delay, with bias **
E1=H(3:2047,2);
E2=H(2:2046,2);
E3=H(1:2045,2);
C1=H(3:2047,3);
C2=H(2:2046,3);
C3=H(1:2045,3);
C=C1;E=E1;
Y=H(4:2048,3);
B=ONES(2045,1);
A=[C1,C2,C3,E1,E2,E3,B];
P=A\Y
a11=p(1,1);a12=p(2,1);a13=p(3,1);
b11=p(4,1);b12=p(5,1);b13=p(6,1);
BIAS=(P(7,1))/(B11+B12+B13)
BB=BIAS*B;
NU=[0 B11 B12 B13];
DE=[1 -A11 -A12 -A13];
[A1 B1 C1 D1]=TF2SS(NU,DE);
EE=E+BB;
X=DSIM(A1,B1,C1,D1,EE');
XX=X';
R2=1-(SUM((C-XX)**2))/SUM(C**2)
```

```
// ** z8d0b; LSE identification using model 8 with a 3 time **
// **
// ** constant delay **
E1=H(3:2044,2);
E2=H(2:2043,2);
E3=H(1:2042,2);
C1=H(6:2047,3);
C2=H(5:2046,3);
C3=H(4:2045,3);
C=C1;E=E1;
Y=H(7:2048,3);
A=[C1,C2,C3,E1,E2,E3];
P=A\Y
A11=P(1,1);A12=P(2,1);A13=P(3,1);
B11=P(4,1);B12=P(5,1);B13=P(6,1);
NU=[0 0 0 0 B11 B12 B13];
DE=[1 -A11 -A12 -A13 0 0 0];
[A1 B1 C1 D1]=TF2SS(NU,DE);
X=DSIM(A1,B1,C1,D1,E');
R2=1-((SUM((C-X)**2))/SUM((C**2)))
```

```
// ** z8d0b; LSE identification using model 8 **  
//  
E1=H(3:2047,2);  
E2=H(2:2046,2);  
E3=H(1:2045,2);  
C1=H(3:2047,3);  
C2=H(2:2046,3);  
C3=H(1:2045,3);  
C=C1;E=E1;  
Y=H(4:2048,3);  
A=[C1,C2,C3,E1,E2,E3];  
P=A\Y  
A11=P(1,1);A12=P(2,1);A13=P(3,1);  
B11=P(4,1);B12=P(5,1);B13=P(6,1);  
NU=[0 B11 B12 B13];  
DE=[1 -A11 -A12 -A13];  
[A1 B1 C1 D1]=TF2SS(NU,DE);  
X=DSIM(A1,B1,C1,D1,E');  
R2=1-((SUM((C-X')**2))/SUM((C**2)))
```

```
// z9d0; LSE identification using model 9 **  
//  
E1=H(4:2047,2);  
E2=H(3:2046,2);  
E3=H(2:2045,2);  
E4=H(1:2044,2);  
C1=H(4:2047,3);  
C2=H(3:2046,3);  
C3=H(2:2045,3);  
C=C1;E=E1;  
Y=H(5:2048,3);  
A=[C1,C2,C3,E1,E2,E3,E4];  
P=A\Y  
A11=P(1,1);A12=P(2,1);A13=P(3,1);  
B11=P(4,1);B12=P(5,1);B13=P(6,1);B14=P(7,1);  
NU=[0 B11 B12 B13 B14];  
DE=[1 -A11 -A12 -A13 0];  
[A1 B1 C1 D1]=TF2SS(NU,DE);  
X=DSIM(A1,B1,C1,D1,E');  
R2=1-((SUM((C-X')**2))/SUM((C**2)))
```